MRAP2 modifies the signaling and oligomerization state of the melanocortin-4 receptor

Iqra Sohail[1]*, Suli-Anne Laurin[2]*, Gunnar Kleinau[3], Vidicha Chunilal[4], Zeynep Cansu Uretmen Kagiali[5], Martin J. Lohse[1,6,7], Patrick Scheerer[3], Michel Bouvier[2], Peter McCormick[4,8#], Paolo Annibale[1,9#], Heike Biebermann[5#]

Affiliations

1 Max-Delbrück-Center for Molecular Medicine, Berlin

2 Institute for Research in Immunology and Cancer, University of Montreal

3 Charité Universitätsmedizin Berlin, corporate member of Freie Universität Berlin and Humboldt-Universität zu Berlin, Institute of Medical Physics and Biophysics, Group Structural Biology of Cellular Signaling, Berlin (Germany)

4 Centre for Endocrinology, William Harvey Research Institute Queen Mary University of London

5 Charité Universitätsmedizin Berlin, corporate member of Freie Universität Berlin and Humboldt-Universität zu Berlin, Institute for Experimental Pediatric Endocrinology

6 ISAR Bioscience Institute, Planegg/Munich

7 Rudolf Boehm Institute for Pharmacology and Toxicology, University of Leipzig

8 Department of Pharmacology and Therapeutics, University of Liverpool and XJTLU-University of Liverpool Joint Centre for Pharmacology and Therapeutics.

9 School of Physics and Astronomy, University of St Andrews

* equal contribution

peter.mccormick@liverpool.ac.uk, pa53@st-andrews.ac.uk, heike.biebermann@charite.de

ABSTRACT

The melanocortin-4 receptor (MC4R) is a G protein-coupled receptor (GPCR) and a key regulator of appetite and metabolism. It can interact with the melanocortin-receptor accessory protein 2 (MRAP2), a single transmembrane helix protein known to interplay with several different GPCRs. However, the consequences of this interaction are not completely understood. Here we report that co-expression of MRAP2 has multiple effects on the MC4R: it enhances G protein-mediated signaling and simultaneously impairs β-arrestin2 recruitment and, consequently, internalization. In addition, co-expression of MRAP2 leads to an increased number of monomers of MC4R by disrupting receptor oligomers. A structural model of the active state MC4R–MRAP2 complex supports the experimentally observed monomerization. Taken together, our data indicate that MRAP2 is an accessory protein that interacts with and influences MC4R structure, biasing its signaling towards G protein-mediated effects.

INTRODUCTION

The melanocortin receptor accessory proteins (MRAPs), namely MRAP1 and MRAP2, are single helix membrane-spanning proteins that have been shown to interact with different G protein-coupled receptors (GPCRs)[1], such as the orexin 1 receptor (OXR1)[2], prokineticin 1 receptor (PKR1)[3] and ghrelin receptor (GHSR1a)[4]. It has been hypothesized that MRAPs act in a similar manner to another family of accessory proteins, called receptor activity-modifying proteins (RAMPs), which associate with numerous class B GPCRs[5-11].

Both MRAP subtypes have been shown to interact with all five members of the melanocortin receptor (MCR) family[12]. MRAP1 is expressed in the adrenal gland and is essential for melanocortin-2 receptor (MC2R) trafficking to the cell surface as well as for adrenocorticotropin hormone (ACTH) binding. MC2R is essentially the sole and indispensable receptor mediating cortisol response to stress[13]. Mutations in MRAP1 as well as in MC2R result in familial glucocorticoid deficiency[14]. Important evidence for this direct structural interaction between MRAPs and class A GPCRs was recently provided by the 3D structure of the active MC2R-G protein complex with ACTH and MRAP1, which was solved by cryo-electron microscopy (cryo-EM)[15]. Functional studies indicated a reduction of MC4R signaling by MRAP1[16].

MRAP2 is predominantly expressed in tissues impacting metabolism and glucose homeostasis, including the central nervous system (CNS), the pancreas, the gut and adipose tissues[17]. Within the mouse CNS, especially in the hypothalamus and in the paraventricular nucleus (PVN), MRAP2 is co-expressed in some neurons together with the MC4R, where it is important for some functions of the MC4R[4,18-20]. Furthermore, MRAP2 and MC4R messenger RNAs were both found in human PVN (The Human Protein Atlas) at a ratio around 3:1 (**Supplementary table 1**). The PVN is a hypothalamic region critical for energy homeostasis and the MC4R is a crucial player in energy metabolism[21]. For that reason, the MC4R is a prime target for potential pharmacological regulation of appetite and body weight[22], as witnessed by more than 160 different pathogenic human variants causing obesity[23].

In addition to rare human heterozygous *MRAP2* mutations that result in increased body weight, mice with global and brain specific *Mrap2* deletion develop marked obesity[4,24]. Moreover, a large-scale study in pigs identified *MRAP2* as a candidate gene associated with daily weight gain, supporting its importance for energy balance in different species[25]. This effect of body weight regulation is further underpinned by a previous study on the role of MRAP2 in zebrafish feeding and growth[26]. In addition to its canonical Gs protein-dependent cell signaling, the MC4R activates the Gq/11 family signaling pathway, which is also involved in appetite regulation[27].

Recent investigations on MRAP2 and MC4R pointed to an increase of signaling by co-expression of both proteins[26,28]. It was hypothesized that the observed increase in Gs-mediated cAMP signaling could be related to MC4R homodimer separation[28]. This scenario, however, has never been explored in detail experimentally, albeit MC4R homodimerization has been reported by us and others, both in human MC4R and in orthologous forms such as *Xiphophorus* MC4R[29-32].

Many questions regarding the mode of action and the resulting effects of the interaction between MRAP2 and MC4R are thus still unclear. In this study, we aimed to investigate the effect of MRAP2 on different MC4R signaling pathways and supramolecular organization, using a suite of fluorescence and bioluminescence resonance energy transfer (FRET and BRET)-based assays, single cell imaging and functional assays[33]. Collectively, our data point to an important role of MRAP2 in modulating the supramolecular organization state of the MC4R, namely its increased monomerization, while directly impacting receptor signaling.

RESULTS

MRAP2 expression increases Gs-mediated cAMP accumulation in the basal and ligand-activated states of MC4R

To investigate the effect of MRAP2 action on MC4R signaling, we first examined the effect of MRAP2 expression on the MC4R-induced Gs activation in heterologously transfected HEK293 cells. Using the Epac-S^{H187} FRET biosensor[34], the increase in cAMP formation was determined as a reduction in FRET between a cyan fluorescent donor and a yellow fluorescent acceptor, and plotted as normalized FRET responses upon stimulation with the agonist α-MSH in the presence or absence of varying ratios of MC4R:MRAP2. In the literature, a wide range of transfection ratios of MRAPs:GPCRs (1:1 to 1:20) with highly variable outcomes are reported, without proper explanation for their selection. Our data show that upon co-expression of either the same DNA mass ratio of MC4R and MRAP2 (1:1, indicated as 1+1), or a fourfold excess of MRAP2 to MC4R (1:4 ratio, indicated as 1+4), there is a leftward shift of the average concentration response curves (**Figure 1A**), reflecting an increase in cAMP production.

Interestingly, both ratios lead to a similar shift in the EC_{50} obtained from fitting the concentration response curves using Hill's equation, namely from 4.5 nM to 1.3 nM, as seen in **Figure 1B**, suggesting a saturable effect. Comparable leftward shift of the concentration-response curves was obtained using another downstream cAMP assay (GloSensor™ technology), but only after 15 minutes of stimulation with α-MSH (**Figure 1C).**

We then determined basal (non-ligand stimulated) cAMP concentrations, in cells transfected with both MRAP2 and the MC4R, as opposed to cells transfected with the MC4R and mock DNA, to keep the DNA content stable. As shown in **Figure 1D**, a sizable increase in basal activity occurs when MRAP2 DNA is transfected in an excess of four parts to one of MC4R DNA. Results are expressed as donor/FRET ratio, which increases proportionally to cAMP formation.

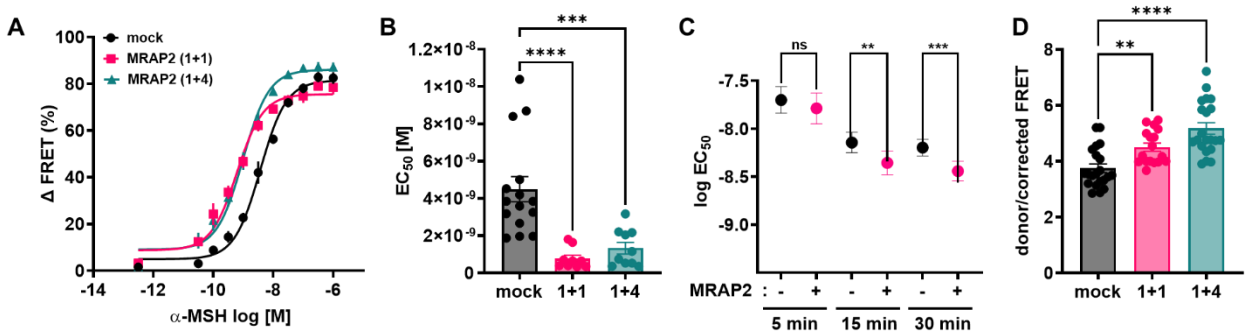

Figure 1: MRAP2 co-expression enhances Gs-mediated downstream signaling of MC4R. (A) Average concentration-response curves of cAMP response upon MC4R stimulation with α-MSH, with and without different amounts of MRAP2 in transiently transfected HEK293 cells. Readout is obtained using the Epac-S^{H187} biosensor. Data are normalized to forskolin response (100%). MC4R is first expressed with an equivalent amount of pcDNA (mock). Plasmid DNA coding for MRAP2 is then co-expressed either in equivalent amounts (1+1) or with a 4-fold higher molar concentration with respect to the MC4R (1+4), always maintaining constant the total amount of DNA transfected. Four independent experiments (with n=8 plate replicates each). **(B)** EC_{50} values across all replicates of concentration response curves obtained using the Epac-S^{H187} FRET biosensor transfected in HEK293 cells, for the three conditions. Mean and SEM are indicated. **(C)** $logEC_{50}$ values from experiments conducted using the cAMP GloSensor assay in HEK293 cells transfected with the MC4R, in the presence or absence of MRAP2 (1+1) for the three time points indicated. **(D)** Basal cAMP values (as assessed by FRET ratio) in the presence or absence of MRAP2 measured using the Epac-S^{H187} FRET biosensor in cells transfected with the Epac-S^{H187} biosensor and different amounts of MRAP2 relative to the MC4R. Mean and SEM are indicated from at least three independent experiments with three plate replicates each. One-way ANOVA as statistical test was performed.

To confirm whether the observations reported in **Figure 1A-C** can be ascribed to enhanced recruitment of the stimulatory heterotrimeric Gs protein at the agonist-bound MC4R, we exploited the nanobody 35 (Nb35), which recognizes the active conformation of $G\alpha_s$, and the miniGs, which binds the active conformation of Gs-coupled GPCR.

In our first assay, a fluorescently labeled Nb35 (Nb35-eYFP), which is known to bind with high affinity the active conformation of the $G\alpha_s$ subunit[35,36], was transfected in HEK293 cells co-expressing SNAP-MC4R (**Figure 2A**). Based on our observations, the addition of an N-terminal SNAP-tag does not affect MC4R downstream signaling (**Supplementary Figure 1**). Total internal fluorescence microscopy (TIRF) was then used to monitor the nanobody recruitment at the plasma membrane of MC4R-expressing cells upon stimulation with 1 µM of NDP-α-MSH. This agonist was employed to maximize our signal-to-noise ratio in these assays, since it is 30 times more potent than α-MSH[37]. Cells were co-transfected with a plasmid coding for $G\alpha_s$ protein to ensure sufficient $G\alpha_s$ in the system to allow detection of the 1:1 stoichiometric recruitment of Nb35 to the receptors. Expression levels of $G\alpha_s$ were also confirmed to be stable in the presence or absence of MRAP2 with a fluorescently tagged version of $G\alpha_s$ (**Supplementary Figure 3**). **Figure 2A** illustrates the enhancement of Nb35 fluorescence (green) at the plasma membrane of SNAP-MC4R-expressing cells (gray) upon agonist addition, in the presence or absence of MRAP2. **Figure 2B** illustrates the kinetics of Nb35 recruitment to the membrane in both cases. Notably, MRAP2 significantly increased the kinetics of nanobody recruitment, suggesting that $G\alpha_s$ recruitment to the receptor and its activation are indeed favored by the action of MRAP2.

In the second assay, MC4R activation at the plasma membrane was confirmed by the increase in the BRET signal between Rluc8-miniGs, which recognizes the active form of $G\alpha_s$-coupled GPCR such as MC4R, and a *Renilla* green fluorescent protein (rGFP) targeted to the plasma membrane with the CAAX box of KRas[38]. The half log-unit leftward shift of the concentration-response curve upon equivalent transfection of MC4R and MRAP2 (1+1) relative to the control mock conditions (**Figure 2C**) confirms that MRAP2 expression favors $G\alpha_s$-coupling (**Figure 2D**). RAMP3, for which no prior indication of an interaction with MC4R has been reported, was used as a negative control, and it indeed showed no effect on miniGs recruitment. In side by side experiments, there is also no change in BRET upon stimulation of cells not transfected with MC4R, showing the response is indeed dependent on this receptor (**Supplementary Figure 4A**).

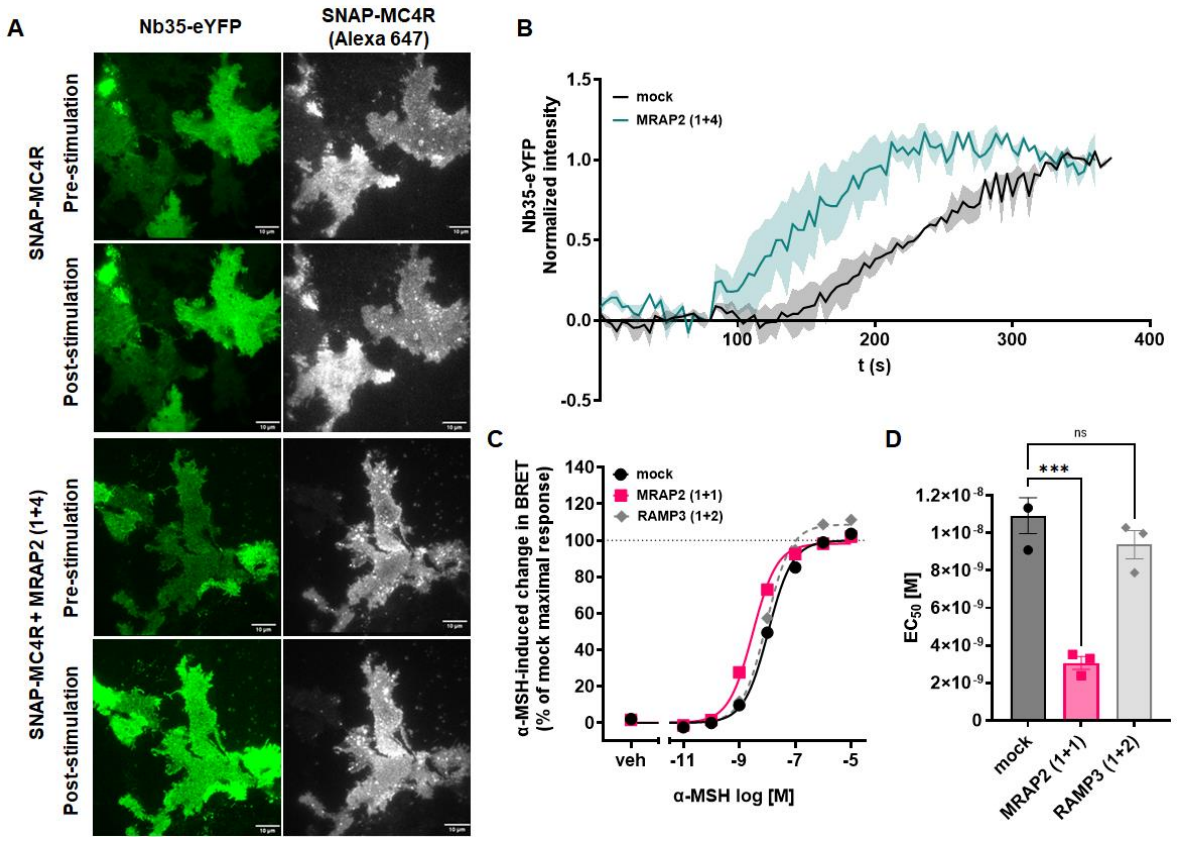

Figure 2: MRAP2 enhances $G\alpha_s$ activation by the MC4R. (A) Representative images from TIRF microscopy of the basolateral membrane of HEK293AD cells expressing SNAP-tagged MC4R labeled using Alexa Fluor 647 (gray) and Nb35-eYFP (green). Images were taken pre- (top) and 4 min post- (bottom) stimulation with 1 µM NDP-α-MSH for cells expressing SNAP-MC4R alone or with MRAP2 (at a ratio of 1:4) and indicate recruitment of Nb35 (green intensity). **(B)** Kinetics of recruitment of Nb35 to the SNAP-MC4R–Gs complex, without (black; 5 transfections, 51 single cells) and with MRAP2 (1+4) (turquoise; 5 transfections, 55 cells). Shown are the normalized fluorescence intensities recorded at the membrane in the eYFP channel; the shaded area represents SEM. **(C)** Mean concentration-response curves of Rluc8-miniGs recruitment to the plasma membrane localization sensor rGFP-CAAX upon MC4R stimulation with α-MSH for 45 minutes, in the presence or absence of MRAP2 or RAMP3, at the indicated ratio with respect to MC4R, in transiently transfected HEK293-SL cells. Normalized data are expressed as mean ± SEM of three independent experiments. **(D)** EC_{50} values from the miniGs recruitment BRET experiments. Data are expressed as mean ± SEM of three independent experiments. Statistical analysis was performed using ordinary one-way ANOVA with Dunnett's multiple comparisons post-hoc test (*** = $p < 0.001$).

MRAP2 increases MC4R-induced activation of Gq signaling pathway

Based on these observations, we further investigated the signal transduction by another G protein that has been shown to be engaged by MC4R, namely $G\alpha_q$, using two different sets of assays.

First, we exploited enhanced bystander BRET between p63RhoGEF, an effector that selectively interacts with activated Gα of the Gq/11 subfamily, and plasma membrane-targeted rGFP[39]. We observed a leftward shift of the concentration response curve upon stimulation with the agonist α-MSH, as well as an increase in the maximal response (E_{max}) (**Figure 3A)**. EC_{50} values were left-shifted by almost one log-unit (**Figure 3B**). In side by side experiments, no response was observed after α-MSH challenge without SNAP-MC4R overexpression, showing that the response is indeed MC4R-dependent (**Supplementary Figure 4D**). The p63RhoGEF sensor is also unresponsive in cells not overexpressing $G\alpha_q$, both in the presence or absence of MC4R, showing that the observed increase in BRET is solely dependent of $G\alpha_q$ and no other G protein in this specific case (**Supplementary Figure 4C**).

Second, we measured second messenger production downstream of $G\alpha_q$ activation. Using IP-One HTRF assay, which monitors inositol monophosphate (IP1) accumulation, a metabolite of inositol-1,4,5-trisphosphate (IP3), this latter being produced following phospholipase C (PLC) stimulation downstream of $G\alpha_q$ activation, we found that MRAP2 co-expression with MC4R yields a leftward-shift in the concentration-response curve of α-MSH (**Figure 3C**). This MRAP2-promoted increase in Gq activation is also supported by NFAT-reporter assays, as a read-out of calcium production, which is typically associated with PLC activation downstream of Gq activation. Overall, co-expression of MRAP2 in a 1+1 (**Supplementary Figure 3**) or 1+4 amount with respect to the receptor, yields a threefold decrease in EC_{50} of IP1 production (**Figure 3D**).

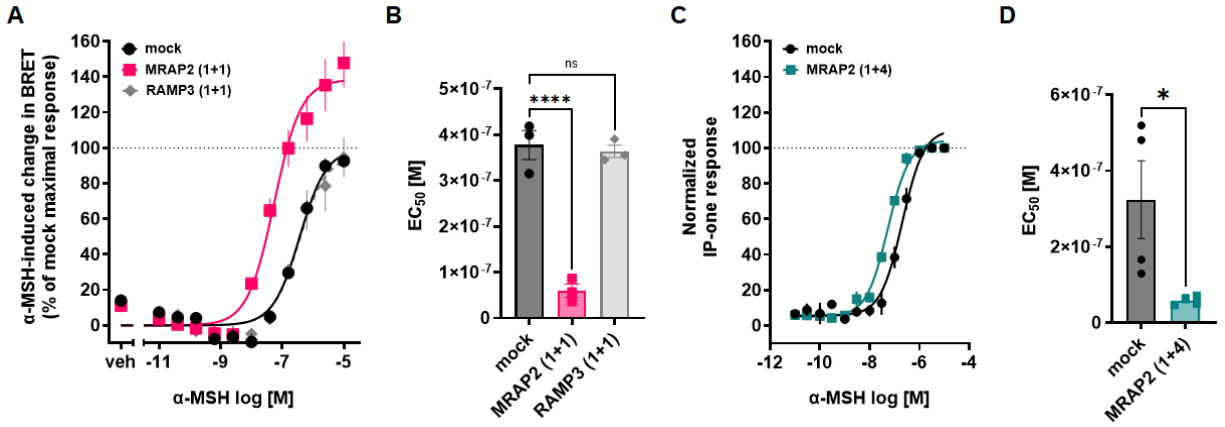

Figure 3: MRAP2 enhances Gq activation. (A) Mean concentration-response curves of the Gq-family selective effector p63RhoGEF-RlucII recruitment to the plasma membrane localization sensor rGFP-CAAX upon MC4R stimulation with α-MSH for 45 minutes, with overexpression of Gq in the presence or absence of MRAP2 or RAMP3 in transiently transfected HEK293-SL cells. MRAP2 or RAMP3 plasmid DNA is co-transfected at the same amount (1:1) with respect to MC4R DNA. **(B)** EC_{50} from the p63RhoGEF recruitment BRET experiments for Gq. Data are expressed as mean ± SEM of three independent experiments. Statistical analysis was performed using ordinary one-way ANOVA with Dunnett's multiple comparisons post-hoc test (**** = $p < 0.0001$). **(C)** Average concentration-response curves of IP-One assay upon MC4R stimulation using α-MSH, with and without MRAP2 1+4 DNA ratio with respect to MC4R, in transiently transfected HEK293T cells. **(D)** EC_{50} values across all the replicates of concentration-response curves for the two conditions. Mean and SEM are indicated. Statistical significance was calculated using an unpaired t-test.

MRAP2 modulates MC4R constitutive and ligand-dependent internalization

It is becoming clear that changes in timing and location of GPCR signaling can alter cell response and physiology[40]. The observation that MRAP2 has such a prominent role in modulating the downstream signaling of MC4R suggests that one potential mechanism for MRAP2 to achieve this modulation might be to influence trafficking of MC4R. This question motivated us to investigate the role of MRAP2 expression in the localization and trafficking of MC4R.

First, we conducted a direct inspection of receptor localization by means of confocal microscopy. Labeling was achieved by a membrane impermeable dye (SNAP Surface Alexa Fluor 647) that irreversibly binds to SNAP-MC4R receptors on the plasma membrane. We then performed a pulse chase experiment that allowed us to monitor any labeled SNAP-MC4R that internalized during a 30-minute incubation period. Next, we compared the cellular distribution of the transfected SNAP-MC4R in HEK293 cells, in the presence or absence of MRAP2 co-expression (1+4). **Figure 4A** displays representative confocal micrographs: when SNAP-MC4R is expressed alone, considerable intracellular fluorescence is evident, due to receptor constitutive internalization during the incubation with the SNAP-tag dye. Notably, the intracellular signal largely disappears when co-expressed with MRAP2. In this case the expression pattern mimics the one observed upon preincubation for 30 minutes with 100 nM AgRP, an inverse agonist that should block constitutive internalization[41]. The use of AgRP in addition to MRAP2 co-expression did not significantly alter this pattern. Thus, it appears that MRAP2 effectively reduces constitutive MC4R internalization.

We then investigated MC4R internalization upon agonist stimulation. In this case, we again used the more potent binding of NDP-α-MSH to maximize the amount of internalized receptor. In HEK293T cells co-expressing SNAP-MC4R and the endosomal marker Cerulean-Rab5 (**Figure 4B, top**), we counted the number of endosomes within the cell before stimulation and 10 minutes after addition of the agonist NDP-α-MSH at saturating concentrations (1µM). In both scenarios, MRAP2 expression decreases significantly the number of endosomes observed per cell (**Figure 4B, bottom**), as quantified in **Figure 4D.** Upon co-expression of MRAP2, there was no effect of NDP-α-MSH on the number of endosomes / cells, suggesting an effective impairment of receptor internalization by MRAP2. This is paralleled by a reduction in the rate of receptor removal from the membrane upon agonist stimulation, illustrated in **Figure 4C.** Additional examples are shown in **Supplementary Figure 5.**

These results were complemented by an internalization readout, exploiting BRET between MC4R-RlucII and an acceptor rGFP fused to the FYVE zinc-finger domain of endofin, which acts as an early endosome targeting sequence (**Figure 4E**)[42]. This approach allowed us to conduct a concentration response readout of MC4R internalization, comparing the effect of co-transfecting increasing amounts of MRAP2. Upon MRAP2 overexpression, either at a 1+1 or 1+4 ratio, there is a clear decrease in the BRET signal within the endosomes **(Figure 4E and 4F)**, again suggesting an impaired ligand-dependent internalization of MC4R in the presence of MRAP2. This is in stark contrast with measurements conducted using RAMP3 as a negative control, where this unrelated accessory protein has no effect on the internalization of MC4R.

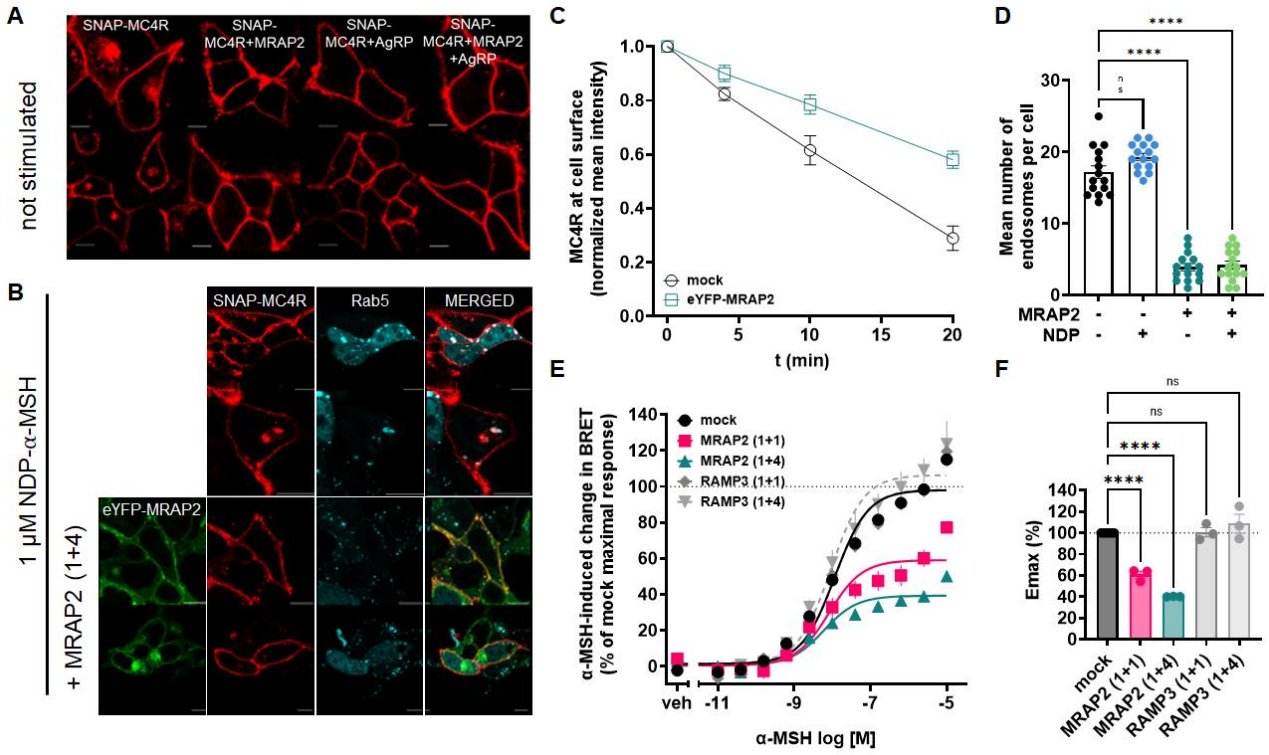

Figure 4: MRAP2 decreases constitutive and ligand-dependent endocytosis of MC4R. (A) Representative confocal micrographs of the localization and trafficking of SNAP-tagged MC4R in basal conditions or after addition of 100 nM of the inverse agonist AgRP for 30 minutes in HEK293T cells. From left to right MC4R: MC4R alone; MC4R in co-expression with MRAP2 (1+4); MC4R alone pre-incubated with AgRP; and MC4R in co-expression with MRAP2 (1+4) pre-incubated with AgRP. More than 3 independent experiments have been done. **(B)** Internalization of SNAP-tagged MC4R after 30 minutes incubation using NDP-α-MSH (1 µM), co-expressed with the endosomal marker Cerulean-Rab5, with or without co-expression of eYFP-MRAP2 (3 transfections, 14 cells). **(C)** Time evolution of SNAP-MC4R intensity at the plasma membrane of cells expressing SNAP-MC4R alone or in co-expression with eYFP-MRAP2 (1+4) upon stimulation with NDP-α-MSH (1 µM). Mean values ± 95% CI of at least three independent experiments and 10 cells. **(D)** Quantification of the number of endosomes per cell detected using Cerulean-Rab5 staining with and without co-expression of MRAP2 (1+4) together with MC4R, both in basal and agonist stimulated conditions (3 transfections – 15 cells). One-way ANOVA has been performed; **** = $p < 0.0001$. Mean and SEM are indicated. **(E)** Mean concentration-response curves of the translocation of MC4R-RlucII to the early endosome localization sensor rGFP-FYVE upon stimulation with α-MSH for 1 hour, in the presence or absence of MRAP2 or RAMP3 in transiently transfected HEK293-SL cells. MRAP2 or RAMP3 plasmid DNA is co-transfected at the same amount (1+1) or fourfold the amount (1+4) of the MC4R-RlucII plasmid DNA. Normalized data are expressed as mean ± SEM of three independent experiments. **(F)** E_{max} values from the translocation to early endosome BRET experiments. Data are expressed as mean ± SEM of three independent experiments. Statistical analysis was performed using ordinary one-way ANOVA with Dunnett's multiple comparisons post-hoc test (**** = $p < 0.0001$).

Overexpression of MRAP2 decreases β-arrestin2 recruitment to the receptor

These results point to both enhanced Gs- and Gq/11-dependent downstream signaling, but, at the same time, a reduced trafficking and internalization rate. The latter led us to investigate if β-arrestin2 recruitment to the receptor, a canonical step following receptor activation that allows for clathrin-mediated endocytic internalization of the receptor for recycling and/or degradation, was affected by co-expression of MRAP2. We employed a luminescence-based protein complementation assay (NanoBiT), whereby luminescence from a complemented luciferase protein is observed upon close proximity of two proteins, in this case the MC4R receptor with a C-terminal fusion and β-arrestin with an N-terminal fusion (see **Methods**)[43].

We observed that overexpression of MRAP2at 1+1 ratio already leads to a significant decrease in β-arrestin2 recruitment directly to the receptor (**Figure 5A**). This reduction of β-arrestin2 recruitment in the basal state parallels the data of reduced constitutive internalization observed in our confocal microscopy quantification (**Figure 4A**). Furthermore, α-MSH stimulation results in reduced β-arrestin2 recruitment in presence of MRAP2 (**Figure 5B**), mirroring the reduction of agonist-dependent MC4R internalization observed in the presence of MRAP2 (**Figure 4B**). These results are again recapitulated in an enhanced bystander BRET assay conducted using a C-terminally labeled β-arrestin2-RlucII and the membrane targeted rGFP-CAAX (**Figure 5C**)[42]. Here, for an equivalent amount of MRAP2 and MC4R transfected (1+1) and a fourfold excess of MRAP2 (1+4), we observed non-statistically significant EC_{50} shifts from approximately 60 nM to 30 nM, whereas substantial drops in E_{max} up to almost 40% were observed. No change in BRET was detected in absence of SNAP-MC4R overexpression, showing the recruitment at the plasma membrane driven by MC4R (**Supplementary Figure 4B**) It is remarkable that, despite the two assays using distinct approaches, and also β-arrestin2 being labeled at both ends (C- or N-terminus), there is an overall agreement between these measurements.

These data suggest that the molecular mechanism of the interaction between MRAP2 and MC4R favors Gs- and Gq/11-coupling, while interfering with internalization, as well as β-arrestin2 coupling.

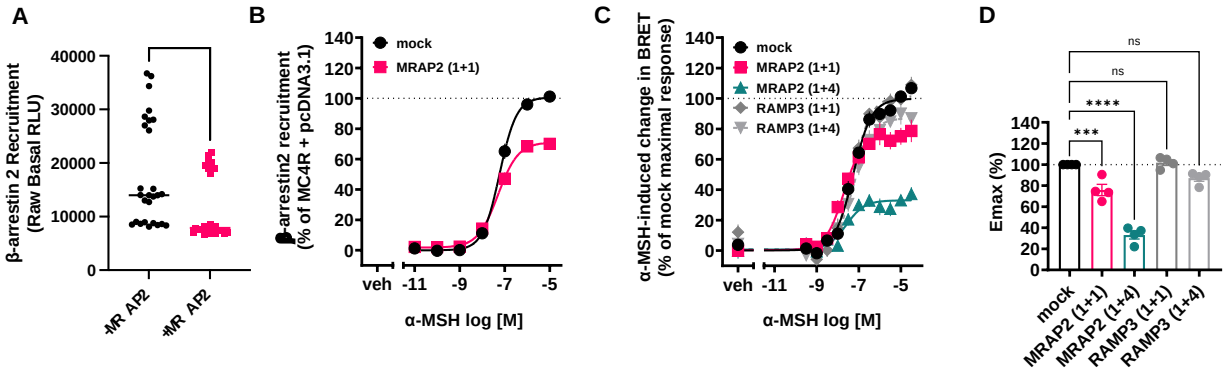

Figure 5: β-arrestin2 recruitment to MC4R in the presence or absence of MRAP2. (A) Bioluminescence-complementation based readout of SmBiT-β-arrestin2 recruitment to MC4R-LgBiT under basal conditions, with and without co-expression of MRAP2 (1+1). **(B)** Concentration-response curve of SmBiT-β-arrestin2 recruitment to MC4R-LgBiT upon α-MSH stimulation with and without co-expression of MRAP2 (1+1). Data represent mean ± SEM from three independent experiments with four replicates each. EC_{50} values and normalized maximal recruitment derived from curve fitting in were 100% and 60 nM ± 8 nM for control condition and 67% and 50 nM ± 8 nM with overexpression of MRAP2 (1+1). **(C)** Mean concentration-response curves of β-arrestin2-RlucII recruitment to the plasma membrane localization sensor rGFP-CAAX upon MC4R stimulation with α-MSH for 2 minutes, in the presence or absence of MRAP2 or RAMP3 in transiently transfected HEK293-SL cells. MRAP2 or RAMP3 plasmid DNA is co-transfected at the same amount (1+1) or fourfold the amount (1+4) of the SNAP-MC4R plasmid DNA (140 ng), with total amount of DNA being constant. EC_{50} values were 58 ± 10 nM, 21 ± 4 nM and 32 ± 8 nM, respectively in the presence or absence of 1+1 or 1+4 MRAP2, and were not significantly different. Normalized data are expressed as mean ± SEM of four independent experiments. **(D)** E_{max} values from the β-arrestin2 recruitment BRET experiments. Data are expressed as mean ± SEM of four independent experiments. Statistical analysis was performed using ordinary one-way ANOVA with Dunnett's multiple comparisons post-hoc test. (*** = $p < 0.001$; **** = $p < 0.0001$).

MRAP2 expression alters the MC4R oligomeric equilibrium towards a monomeric state

Receptor oligomerization has long been a mechanism invoked to explain the modulation of GPCR downstream signaling, although less commonly this has been shown to influence the ligand-dependent response or to be in turn influenced by ligands[44]. Based on BRET-based studies, we have previously suggested that the MC4R has a homodimeric arrangement[29], which can impact downstream signaling of the receptor, in particular coupling to Gs and Gq.

Thus, we tested the hypothesis that co-expression of MRAP2 can modulate the oligomeric state of MC4R. For this purpose, we performed a single-cell assay based on molecular brightness, similar to that used for other GPCRs[45]. We first conducted confocal microscopy of the basolateral membrane of cells expressing different receptor N-terminally tagged with SNAP-tag (**Figure 6A**). The β1-adrenoreceptor (SNAP-β1AR) brightness mean was identified as a monomeric reference. As a reference for the dimeric state, we employed C-X-C chemokine receptor type 4 (SNAP-CXCR4), which we and others have identified as largely dimeric at the concentrations found in heterologously expressing systems[44,46] (**Supplementary Figure 6**). The fingerprint of the SNAP-MC4R, with respect to these two controls, is that of a largely dimeric receptor, with the presence of some higher order oligomers, leading to brightness values more than 0.4 (more than twice the monomeric brightness of 0.2 observed in the SNAP-β1AR) (**Figure 6B**). However, co-expression of MRAP2 (1+4) strikingly leads to a radical change in the MC4R oligomeric fingerprint, and largely monomerizes the receptor. Furthermore**,** MRAP2 does not appear to increase the average number of heterologously expressed MC4Rs at the plasma membrane of the cell (**Supplementary Figure 7A**), as reported by enhanced bystander BRET assays. Moreover, the effect does not seem to be dependent on the actual stoichiometry between the two proteins (**Supplementary Figure 7B**).

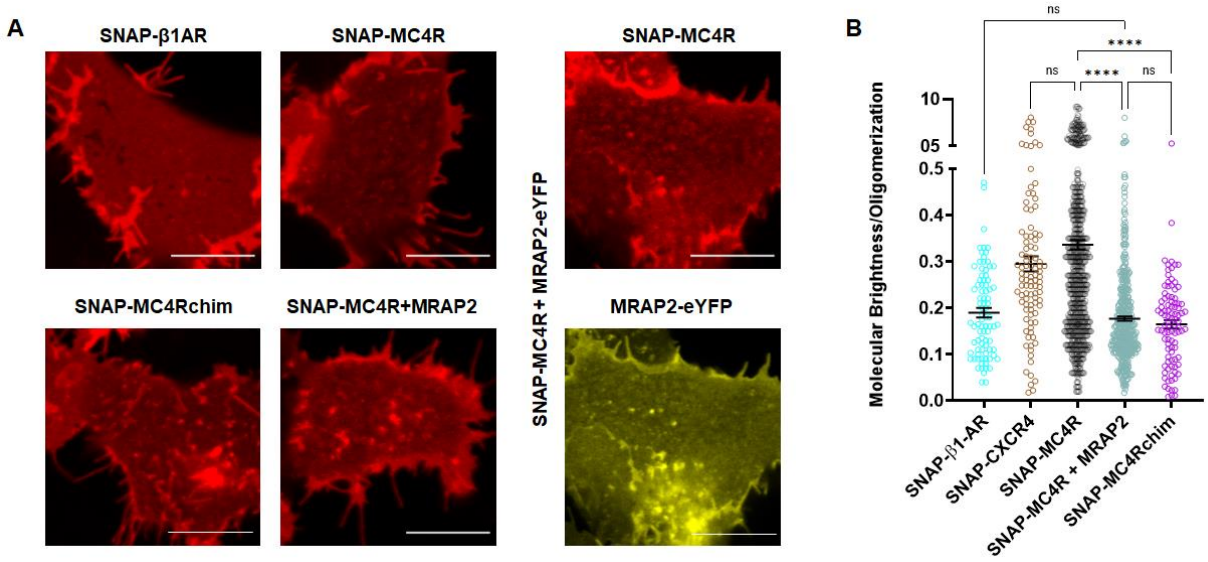

Figure 6: Oligomeric state of MC4R in the presence or absence of MRAP2. (A) Representative confocal micrographs of the basolateral membrane of HEK293 cells expressing SNAP-tagged GPCRs, all labeled using Alexa 647. From the top left the SNAP-β1AR (3 transfections, 13 cells), SNAP-MC4R (44 cells, 6 transfections), SNAP-MC4R in combination with eYFP-labeled MRAP2 (as a reference), SNAP-MC4R in presence of untagged MRAP2 (3 transfections, 15 cells), and finally the SNAP-MC4Rchim (3 transfections, 18 cells). **(B)** Molecular brightness values obtained for each of the control groups listed in **A**. Each dot represents a value from a ROI within a cell. One-way ANOVA has been performed; **** = $p < 0.0001$. Mean ± SEM are shown in black.

Chimeric MC4R that can not homodimerize mimics MRAP2 effect on signaling

Our data delineate a scenario in which the MC4R is predominantly expressed as a dimer that disassembles into a monomer upon interaction with MRAP2. This is accompanied by an increase in Gs and Gq activation, an elevated downstream cAMP and IP3 production, a decrease in β-arrestin2-mediated recruitment, and a significant reduction in receptor internalization. This suggests that MC4R monomerization influences the receptor towards G-protein coupling, including both Gs and Gq, as opposed to β-arrestin2.

We tested this hypothesis by examining the oligomerization behavior of a specific MC4R chimera (SNAP-MC4Rchim), that was previously engineered by replacing the intracellular loop 2 (ICL2) of MC4R with that of the cannabinoid 1 receptor (CB1R). We have previously shown that this chimera has impaired homodimerization by BRET-based assay[29], and it also displays a monomeric fingerprint in our molecular brightness assays (**Figure 6B**). The expression of MRAP2 was confirmed using a red fluorescent reporter (mRuby2), expressed in the cytosol of those cells containing the MRAP2 plasmid.

We then tested the function of this chimera using the Epac-S^{H187} FRET biosensor (**Figure 7A**). Notably, the absolute maximal for cAMP production for this chimeric receptor is increased compared to wild-type (WT) MC4R (**Figure 7A**), and the EC_{50} is decreased (**Figure 7B**)In these measurements, the data were not normalized to highlight the significant increase in constitutive activity of this chimeric receptor. This effect is in line, albeit larger, than what is observed for the WT MC4R upon co-expression of MRAP2, as reported in **Figure 1D**. Interestingly, the effect of the chimera on the EC_{50} corresponds to that observed when co-expressing MRAP2 with the wild-type MC4R (see **Figure 7B**)**,** suggesting that the lower EC_{50} could in part be due to the receptor being in a monomeric state.

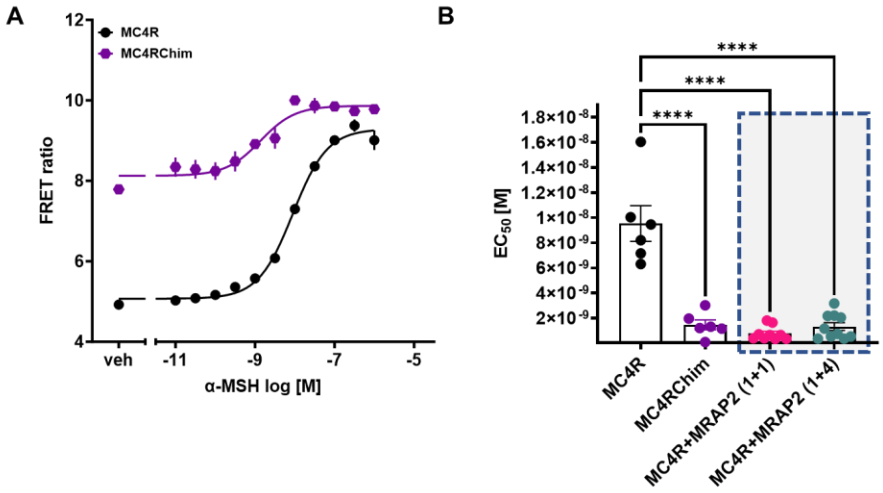

Figure 7: The monomeric MC4Rchim chimera increases MC4R Gs-mediated signaling. (A) Average concentration-response curve of cAMP response against α-MSH using the Epac-S^{H187} FRET biosensor in transiently transfected HEK293 cells expressing SNAP-MC4R and chimeric variant of MC4R containing the ICL2 of the CB1R (MC4Rchim), which is a monomer. MC4RChim exhibits a higher constitutive activity increased cAMP response comparable to co-expression of MRAP2; at least three independent experiments with three replicates each. **(B)** EC_{50} values across all the replicates of concentration response curves obtained using the Epac-S^{H187} FRET biosensor transiently transfected into HEK293 cells, for each condition. Dashed rectangle highlights data taken from Figure 1 for comparison. Mean and SEM are indicated, and one-way ANOVA has been performed; **** = $p < 0.0001$.

Putative MC4R–MRAP2 interaction sites

In order to understand how a MC4R-monomer/MRAP2 complex might be constituted and impact receptor dimerization and signaling, we generated a structural homology model of an active MC4R–MRAP2–Gs protein complex with an agonistic ligand. To do so, we used the recently determined ACTH–MC2R–MRAP1–Gs protein complex (PDB ID: 8GY7)[15] and the NDP-α-MSH–MC4R–Gs protein complex (PDB ID: 7PIV)[36] as structural templates. The observed binding interface between MRAP1 and MC2R could be assumed to be the same between MRAP2 and MC4R, as it is in principle conserved for all feasible MCR subtype-MRAP1 complexes[12,47] because of high conservation in the sequences of the receptor group (MC4R/MC2R ~60%, MC4R/MC5R ~70%, MC4R/MC3R ~60%, MC4R/MC1R ~60%), and between MRAP1 and MRAP2 (**Supplementary Figure 8**). Furthermore, ACTH binds with high affinity to the human MC4R *in vitro* when MRAP2 is co-expressed[48]. This suggests MC4R-MRAP2 interactions and the relative spatial adjustment to each other could be similar to what is observed in the structure of the MC2R-MRAP1 complex. Here, the N-terminus of MRAP1 specifically interacts with ACTH, likely increasing receptor affinity for ACTH, which critically depends on the overall orientation between MRAP and the receptor. Based on this structure, the predicted MC4R-MRAP2 heteromer interface is constituted mainly by interactions between the receptor transmembrane helix 5 (TMH5), the receptor TMH6 and the MRAP2 membrane-spanning helix (magenta arrows in **Figure 8**). Further interaction sites are predicted to be between the receptor TMH7and extracellular loop 3 (ECL3) transition and the receptor N-terminal tail (Ntt) with the MRAP2 Ntt and the MRAP2 membrane-spanning helix. In consequence, this supposed heteromeric receptor-MRAP2 complex could affect MC4R homo-oligomerization by sterically covering putative receptor-receptor interaction sites, mainly at TMH5-TMH6. Indeed, TMH5 and TMH6 were reported to be in the homodimerization interface of certain GPCRs, like CXCR4[49] or the μ-opioid receptor (μOR)[50]. This region of MC4R is thus a leading candidate amongst the potential sites to modulate the equilibrium of the monomeric and dimeric state.

Of particular note, structural information on the MC2R–MRAP1 complex does not include the full-length MRAP1, because the complete intracellular C-terminal tail is missing, which excludes any prediction of a potential impact on receptor function such as G-protein coupling or homodimerization.

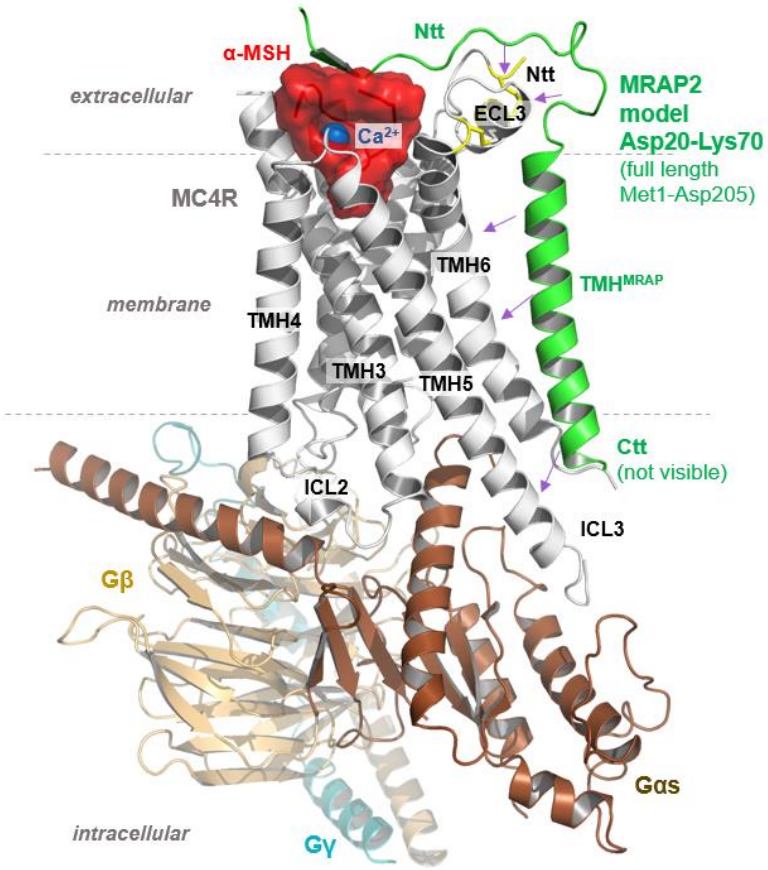

Figure 8: Structural interaction model of MC4R and MRAP2. In this model α-MSH (red surface) interacts with the MC4R between the transmembrane helices (TMH) and interconnecting extracellular and intracellular loops (ECL and ICL) as described recently[36], together with the essential co-binding factor calcium (blue sphere). The heterotrimeric Gs protein couples intracellularly at the agonist bound MC4R conformation. MRAP2 (green) contacts to MC4R are supposed at TMH5, TMH6, ECL3 and the N-terminus (Ntt). Arrows indicating putative interaction sites between receptor and MRAP2.

DISCUSSION

In this study, we have provided novel insight into the molecular mechanisms that underlie the action of MRAP2 on MC4R cellular function. Using real-time signaling assays, single molecule microscopy approaches, and molecular modeling we demonstrate: (*i)* that MRAP2 enhances MC4R signaling for at least two different G protein-driven signaling pathways; *(ii)* that MRAP2 modulates MC4R cellular trafficking, and *(iii)* that MRAP2 modulates the oligomeric state of MC4R, which appears to have a direct impact on its function[11]. These findings shed light on how MRAP2 has a direct and modulatory influence on the MC4R, and thus represents a potential keystone in MC4R-associated functions such as energy consumption or appetite regulation.

The identification of the first human *MRAP2* mutations found in obese patients highlighted the role of MRAP2 in modulating MC4R signaling[4,24,28]. It was presumed that MRAP2 would function analogously to RAMPs, that can modulate GPCRs by influencing their trafficking to the cell surface, expression, ligand binding, signaling and internalization. Towards this end, an intense effort has been undertaken to understand the role of MRAP2 on these aspects of MC4R physiology and function. In particular, a role of MRAP2 in reducing the capacity of MC4R to form dimers/oligomers was speculated, but until now not experimentally validated[29].

Our findings that MRAP2 increases the capacity of MC4R to activate different G protein subtypes begs the questions (*a*) is this a true reflection of physiology and (*b*) how this might be achieved. In support of the former, there is a precedent for these findings in previous studies that demonstrated a reduction of MC4R signaling in the presence of loss-of-function MRAP2 mutations[4,24,28]. In addition, a more specific increase in Gs and Gq activation by MC4R was observed in HEK293 cells that stably express MRAP2[51]. Interestingly, we could also detect a major increase in signaling with $G\alpha_{15}$, another G protein from the Gq/11 family (**Supplementary Figure 4D**). Furthermore, PTX-sensitive activation of endogenous MC4R in GT1-7 murine hypothalamic cell-line was already described, suggesting that Gi activation can be detected in some systems[52]. It would be interesting to see the impact of MRAP2 on Gi pathways.

The potential mechanisms behind the increase in G protein signaling are still opaque, but can be inferred by some of our additional findings in this study. For example, our discovery that there is a decrease in β-arrestin2 recruitment suggests that there could be less desensitization of the receptor. Reduced β-arrestin2 binding and less desensitization would in turn favor increased G protein signaling, as there would be more receptors available to bind and activate G protein complexes. We also found that the effects of MRAP2 co-expression are not limited to a potentiation of G protein-dependent signaling, but also impact downstream processes, such as receptor trafficking. Thus, reduced β-arrestin2 recruitment would lead to decreased internalization, as previous research has indicated that MC4R endocytosis is entirely dependent on β-arrestin recruitment[12]. This would typically result in a buildup of receptors at the cell surface, enhancing G protein signaling responsiveness, albeit our measurements do not seem to reflect a MRAP2-dependent change in MC4R expression level at basal state (**Supplementary Figure 7**), suggesting that other mechanisms could be further at play.

Beyond the effects of altered receptor trafficking, we found that MRAP2 was able to impact the MC4R monomer-dimer equilibrium. This effect of MRAP2 introduces another potential scenario whereby the MC4R monomer could exhibit a heightened ability to interact with G proteins compared to the homodimer. This could be due to (1) an increase of signaling protomers due to the breakage of the MC4R homo-oligomers, (2) a modulation of the MC4R protomer signaling by the specific interaction with MRAP2 or (3) a combination of both effects. Our current data using the MC4R chimera (**Figure 7**) appear to support the first hypothesis.

The hypothesis that the oligomer state influence the function of the receptor was previously suggested for the β2-adrenergic receptor (β2AR)[53,54]. Interestingly, a correlation between GPCR monomer-dimer populations and β-arrestin has already been reported, in which GPCR dimerization has been shown to impact β-arrestin interaction[55]. These possibilities shed light on the intricate mechanisms underlying GPCR signaling regulation and warrant further investigation. Taken together, these data provide compelling evidence that MRAP2 has G protein-dependent and independent action on MC4R signaling. In order to understand at the molecular level how MRAP2 could achieve such an impact on MC4R, we developed a homology model between MRAP2 and MC4R. This model indicates potential interaction sites between MRAP2 and MC4R at TMH5, TMH6 and the TMH7-ECL3 transition (**Figure 8**). While so far it is unknown how MC4R homodimers are exactly constituted, TMH5 and TMH6 have already been identified from various GPCR-GPCR dimer structures as potential interaction sites between the protomers[56], as in the CXCR4 homodimer (PDB ID: 3ODU[49]), or the μOR homodimer (PDB ID: 4DKL[50]). In consequence, binding of MRAP2 at this region should compete with dimerization (or oligomerization) of MC4R. The subsequent monomerization would lead to a receptor-G protein stoichiometry of 1:1 (increased capacity), instead of 2:1 in the receptor dimer-G protein complex. Such a 2:1 ratio is already known from the cryo-EM structure of the active state dimeric apelin receptor (PDB ID: 7W0N[57]). Of note, TMH5 and TMH6 of GPCRs are hot-spots in structural rearrangements during receptor activation[58], with the highest degree known for TMH6[58], and our MC4R–MRAP2 model suggests an interaction of both receptor helices with the single helix of MRAP2. However, this putative interaction has no negative or direct effect on the binding of the G protein to the MCRs, as evidenced by the stable binding of the G protein to the MC2R monomer or the G protein-associated signaling increases observed in this current study.

In contrast, all GPCR-arrestin structural complexes known to date lack a structurally resolved intracellular loop 3 (ICL3) (except in the rhodopsin-arrestin complex). In addition, there is no outward orientation of the intracellular TMH5 ends, as is clearly seen in the MRAP1–MC2R–Gs complex. The TMH5-ICL3-THM6 axis is presumably important for the spatial adjustment of the arrestin at the receptor, which, according to current knowledge, has a higher structural variability[59]. MRAP2 could thus influence the binding of the arrestin as an interfering factor, an aspect that has already been suggested for PKR1[3]. The interaction of the TMH5-ICL3-TMH6 axis by MRAP2, on the other hand, probably further implies an increased retention of the active state, which might allow for better G-protein coupling[55]. However, this hypothesis needs to be substantiated by new structural findings such as a MC4R–MRAP2–G protein complexes, a MC4R homodimers or a MC4R–arrestin complex.

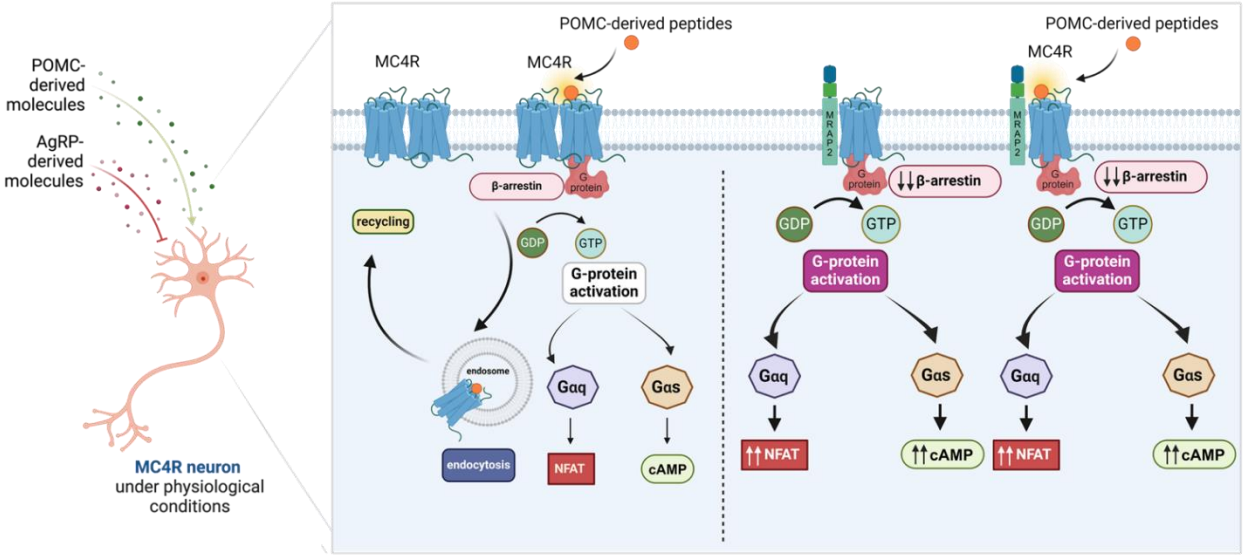

Figure 9: Effects of MRAP2 at the MC4R. The MC4R is activated by POMC-derived peptides from POMC-neurons the nucleus arcuatus, left side. In addition, AgRP/NPY neurons of the nucleus arcuatus produce AgRP which is in turn axonally transported to the PVN where the function of the MC4R is modulated by AgRP and POMC-derived peptides. Constitutively, the MC4R is a homodimer at the plasma membrane of cells (square, left side). As such, it can interact with Gs and Gq as well as β-arrestin2, both constitutively as well as in response to POMC-derived molecules such as α-MSH and result in internalization. Upon co-expression of MRAP2 (square, right side), the dimer is broken, and the basal (condition in the middle) as well as the ligand-dependent (condition on the left side) Gs and Gq interaction is enhanced, whereas ligand-dependent β-arrestin2-recruitment is impaired. These processes are further accompanied by a reduction in constitutive and ligand-dependent internalization.

Final remarks

In summary, our results demonstrate the important role of MRAP2 in modulating MC4R signaling cascades in response to stimulation by the endogenous agonist α-MSH, as well as its synthetic analog NDP-α-MSH, and the connection of these effects to alterations to the monomer-dimer equilibrium. Albeit monomerization of MC5R by interaction with MRAP1 has been previously shown[60], our observations at MC4R are new experiments that directly show an effect of MRAP2 in regulating an oligomeric GPCR state, which has not been shown experimentally before. Moreover, our data also reveal the enhanced downstream signaling effect of a monomeric receptor compared to a dimer, which is an important progress considering that only a handful of studies have provided evidence for an effect of the oligomeric state on downstream signaling[61].

Considering these results at the physiological level, MRAP2 expression can play an important role in the modulation of cellular signaling. Here the important question would be what modulates MRAP2 expression in those cell types or neurons that express MC4R over an individual's lifetime and if MRAP2 expression is modulated in times of famine of food surplus. Although we did not observe a significant difference in terms of the varying relative expressions of MRAP2 and MC4R, a reduction in MRAP2 expression relative to a 1:1 stoichiometry could have a profound impact on MC4R pharmacology and thus physiology *in vivo*. Cell-type specific expression of MRAP2 emerges thus as an additional tool that organisms can use to modulate and bias GPCR signaling in a context-dependent fashion[20]. In addition, more aspects of MRAP2 besides monomerization might exist. For example a role of MRAP2 in cilial localization of MC4R was recently reported that is supposed to be critical for MC4R function[20].

Taken together, our results point to a more complex physiological system for the regulation of MC4R-mediated pathways controlling metabolism and satiety, which we expect to be reflected also at the neuronal level. Our data pave the way to test this concept for other GPCRs where signal modulation through interaction with either MRAP1 or MRAP2 has been observed[1].

Acknowledgments

We thank Sabine Jyrch for excellent technical assistance. We would like to thank Alexei Sirbu for his helpful support. This work was supported by the Deutsche Forschungsgemeinschaft (DFG) (German Research Foundation) through SFB1423, Project-ID 421152132, subprojects C03 (to P.A., M.J.L), B02 (to H.B.), A01/Z03 (to P.S.). Funding was received through Germany's Excellence Strategy – EXC 2008 – 390540038 – UniSysCat (Research Unit E) (to G.K. and P.S.) and by the European Union's Horizon 2020 Research and Innovation Programme under the Marie Skłodowska-Curie grant agreement No 956314 [ALLODD] (to P.S.). UKRI funding to P. McC. CIHR funding (PJT-183758) to M.B. FRQS PhD scholarship to S-A.L.

Author Contributions

H.B., P.McC, M.B. and P.A. designed research

I.S., S-A.L, V.C., A.S., Z.C.U.K., P.S., G.K. performed research

I.S., S-A.L, V.C., P.A., Z.C.U.K, H.B., M.B. data analysis

G.K. and P.S. performed, analyzed and visualized structure and sequence analysis

I.S., V.C., P.A., H.B., graphical analysis

I.S., H.B., P.McC., G.K., P.S., M.J.L, P.A., S-A.L M.B. wrote and revised the manuscript

H.B., P.McC., P.A., M.B. supervision of experiments

H.B., P.A., M.J.L., P.S., M.B funding acquisition

SUPPLEMENTARY MATERIALS

Supplementary Figures and Tables

Protein	nTMP	MC4R:MRAP2
MC4R	3.6	1:3
MRAP2	11.5	

Supplementary Table 1: The normalized gene expression values (nTMP) representing the RNA expression of the MC4R and MRAP2 in the paraventricular nucleus of the hypothalamus (The Human Protein Atlas, 2023). The values obtained give an expression ratio for MC4R to MRAP2.

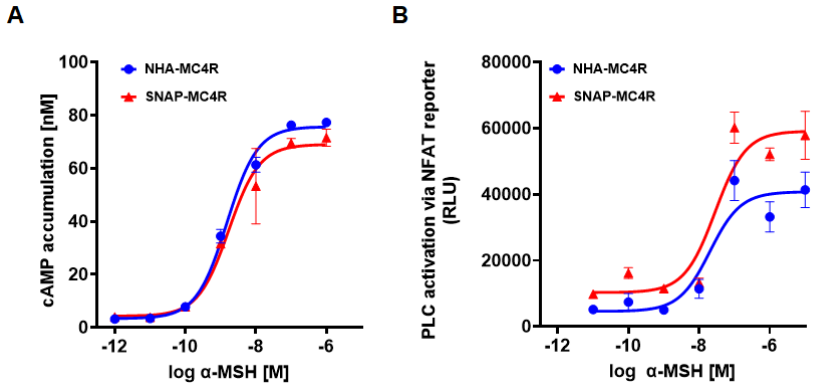

Supplementary Figure 1: N-terminal SNAP tag does not affect MC4R downstream signaling. (A) cAMP accumulation or **(B)** PLC activation in cells co-transfected with NFAT reporter cells were stimulated with increasing amounts of α-MSH and cAMP accumulation or NFAT-induced luminescence were determined (**Materials and Methods**).

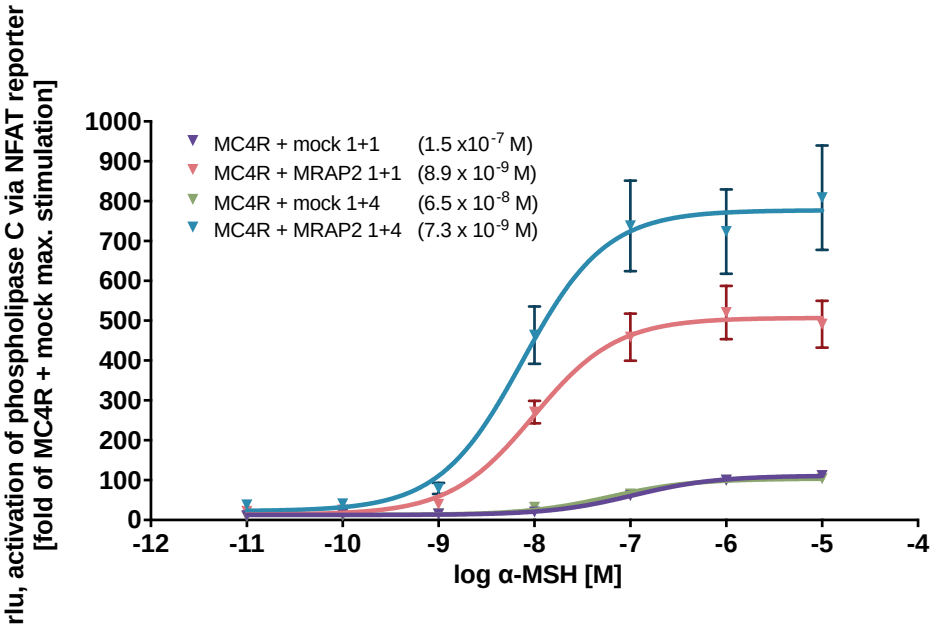

Supplementary Figure 2: Activation of phospholipase C activation via NFAT reporter gene assay. In order to determine the effect of MRAP2 on phospholipase C activation MC4R and indicated ratios of MRAP2 and NFAT reporter were co-transfected into HEK293 cells. 48 h after transfection cells were stimulated with increasing amounts of α-MSH for 6h and luciferase activity was determined. The result of 8 independent experiments performed in triplicates is shown.

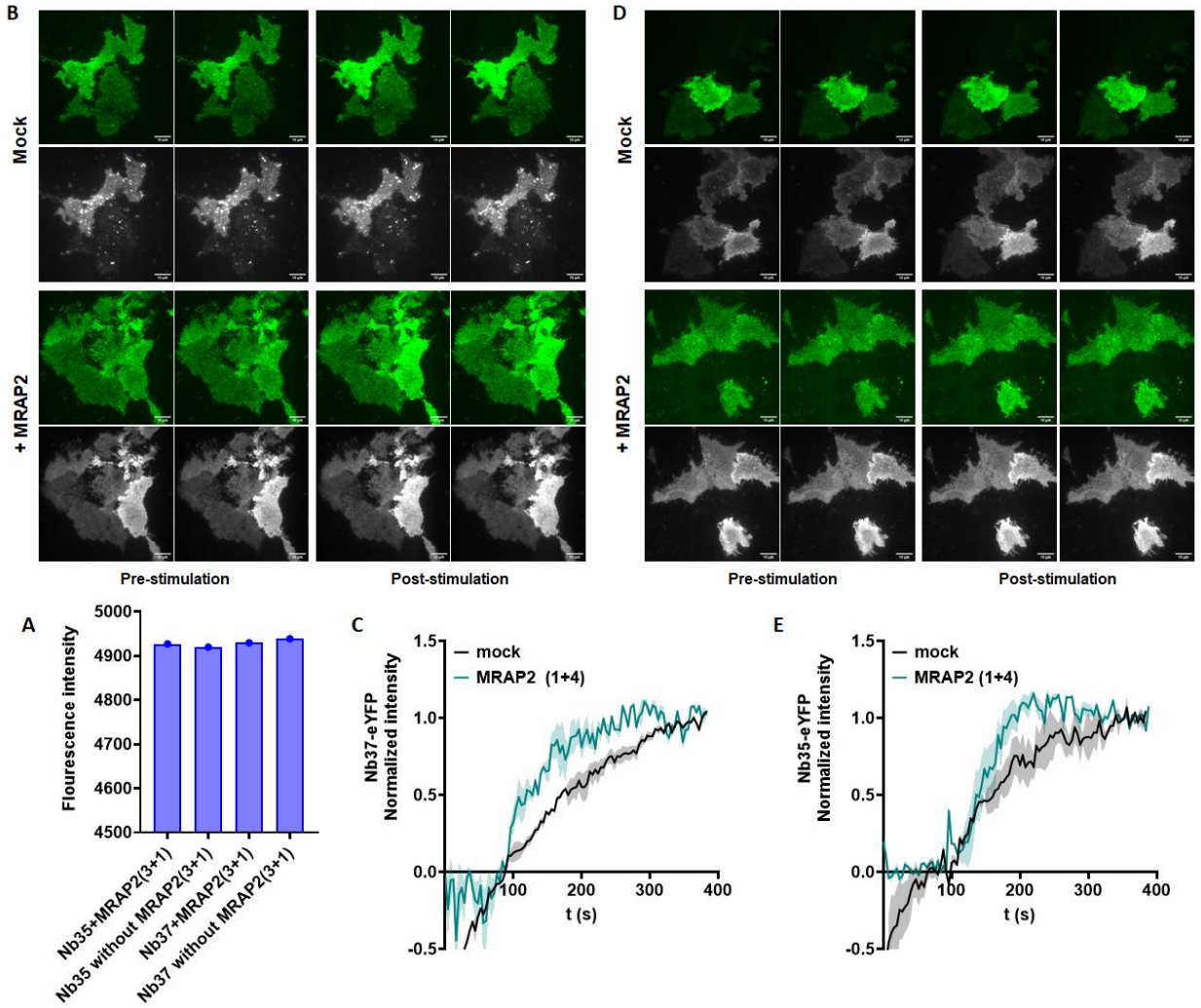

Supplementary Figure 3: Recruitment of Nb35 and Nb37 in HEK293 cells heterologously expressing SNAP-MC4R +/- MRAP2 and Gs. (A) Fluorescence intensity (arbitrary intensity units) in the cyan channel from populations of cells co-transfected with Gs-CFP plasmid and the constructs indicated. No fluctuation in the expression level of $G\alpha_s$ is observed. **(B)** Recruitment of Nb35-eYFP to Gs-positive cells with and without MRAP2. SNAP-MC4R labeled with SNAP-Surface 647 (gray) and Nb35-eYFP (green). **(C)** Kinetic of the intensity of Nb35-eYFP measured at the plasma membrane of HEK293AD cells using TIRF, with and without MRAP2. **(D)** Recruitment of Nb37-eYFP to Gs-positive cells with and without MRAP2. SNAP-MC4R labeled with SNAP-Surface 647 (gray) and Nb35-eYFP (green). **(E)** Kinetic of the intensity of Nb37-eYFP measured at the plasma membrane of HEK293AD cells using TIRF, with and without MRAP2.

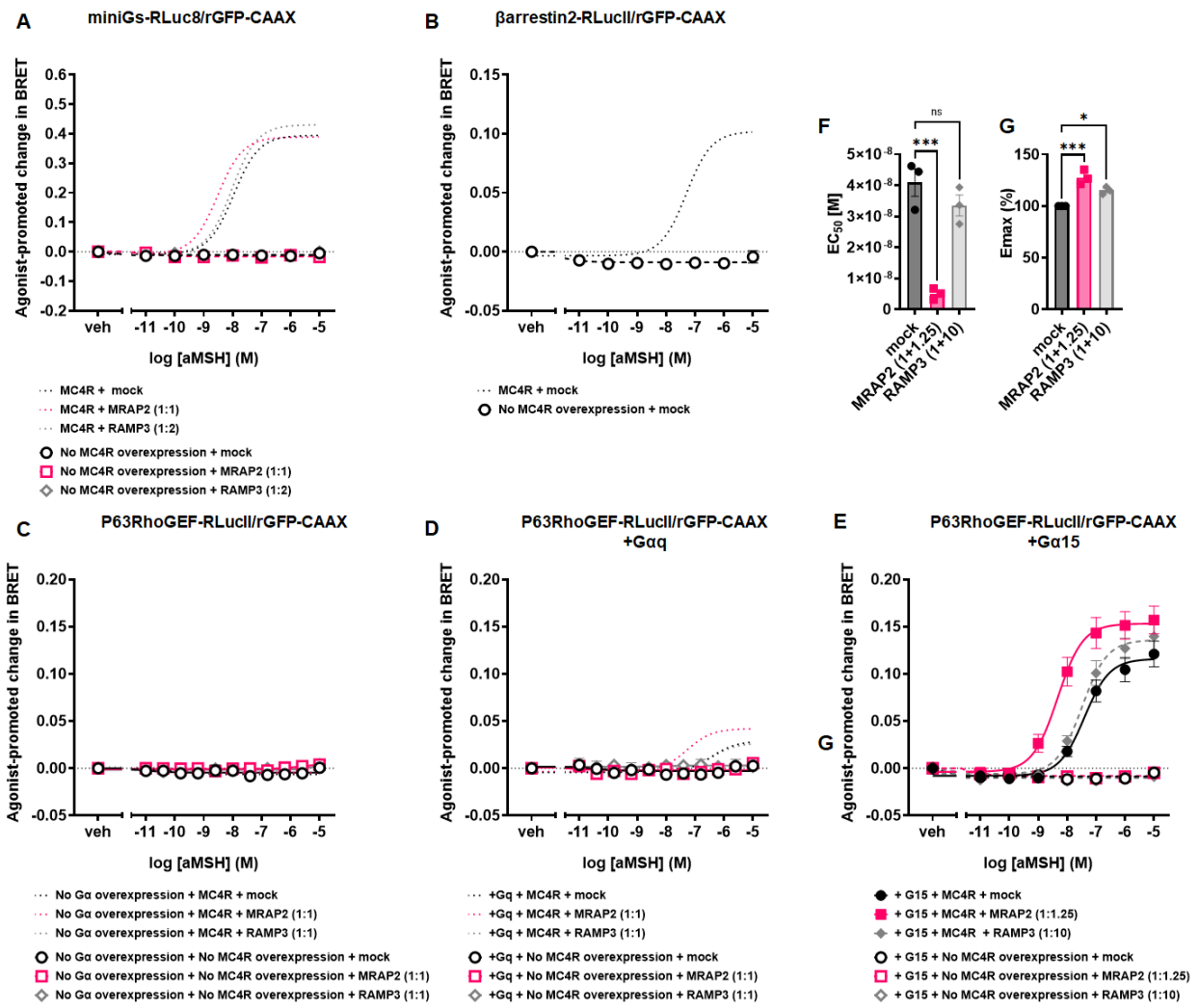

Supplementary Figure 4: Complementary BRET experiments. Mean concentration-response curves of BRET sensor stimulation with α-MSH, without or with overexpression of SNAP-MC4R in the same set of experiments unless stated otherwise, in the presence or absence of MRAP2 or RAMP3 at the indicated ratio with respect to MC4R, in transiently transfected HEK293-SL cells. Baseline-corrected (agonist-promoted change in BRET) responses are expressed as mean ± SEM of three independent experiments. **(A)** Rluc8-miniGs recruitment to the plasma membrane localization sensor rGFP-CAAX after 45 minutes of stimulation. Curves from Figure 2C are represented in dotted lines for scale reference. **(B)** β-arrestin2-RlucII recruitment to the plasma membrane localization sensor rGFP-CAAX after 3 minutes of stimulation. This experiment was carried independently of the one presented in the main text. **(C-E)** Gq-family selective effector p63RhoGEF-RlucII recruitment to the plasma membrane localization sensor rGFP-CAAX after 45 minutes of stimulation, **(C)** in the presence or absence of overexpression of **(D)** $G\alpha_q$ or **(E)** $G\alpha_{15}$. Curves from Figure 3A are represented dotted lines for scale reference in panel D. **(F)** EC_{50} and **(G)** E_{max} from the p63RhoGEF recruitment experiments for Gq. Data are expressed as mean ± SEM of three independent experiments. Statistical analysis was performed using ordinary one-way ANOVA with Dunnett's multiple comparisons post-hoc test.

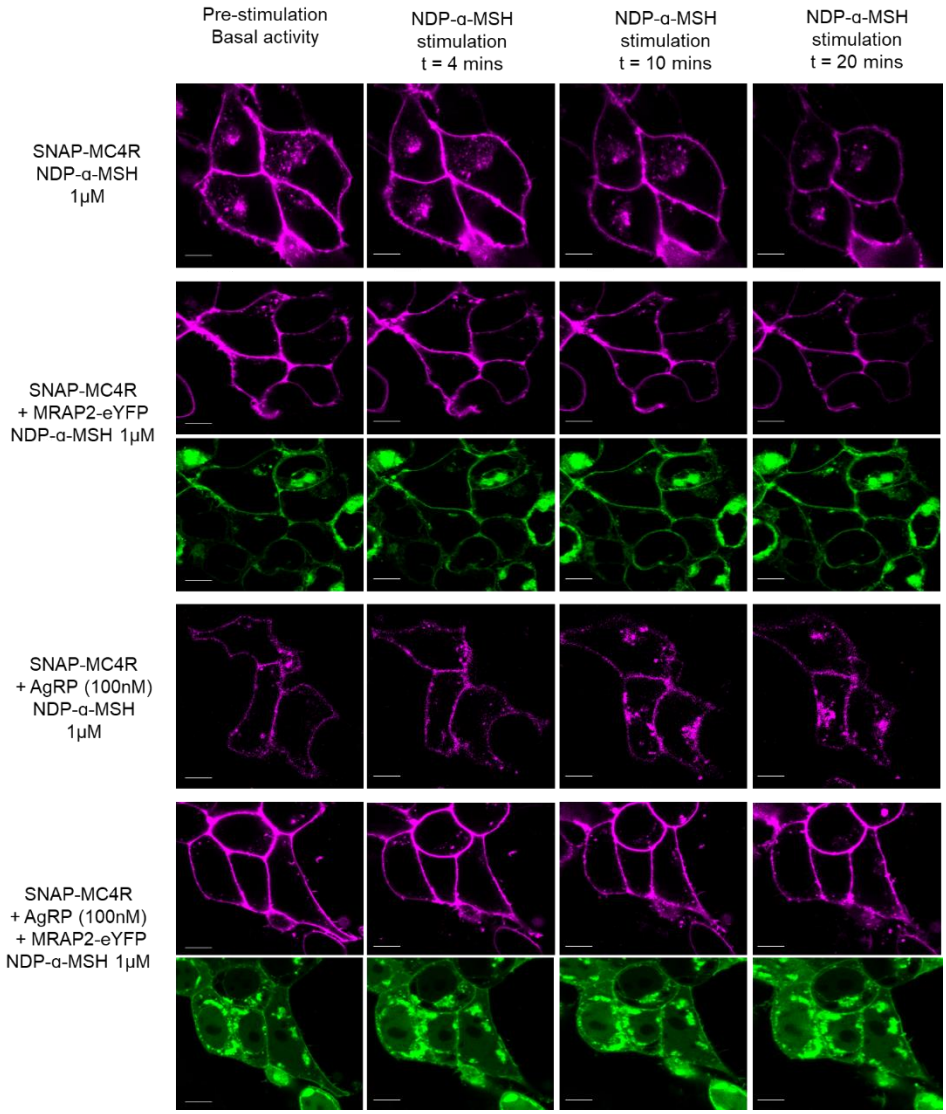

Supplementary Figure 5: Internalization of SNAP-MC4R with and without expression of MRAP2. From top to bottom, confocal micrographs of SNAP-MC4R together with eYFP-MRAP2, when indicated. Evolution of MC4R and MRAP2 cellular localization at four timepoints, before and respectively after 4, 10 and 20 minutes after the addition of 1μM NDP-α-MSH. In the last two rows cells expressing the receptor are further preincubated with 100 nM AgRP to suppress constitutive internalization.

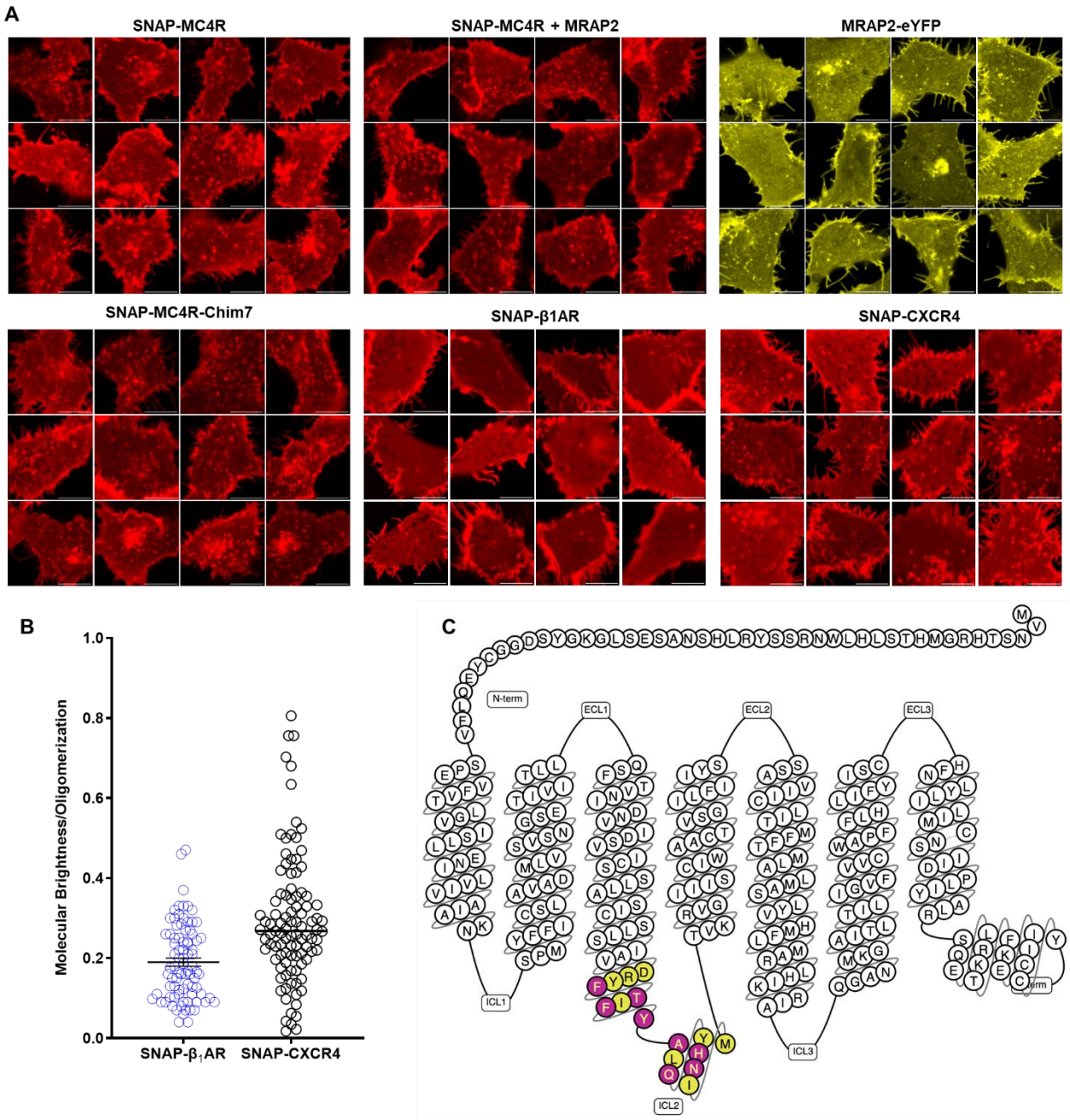

Supplementary Figure 6: Control datasets for molecular brightness experiments. (A) Representative confocal micrographs of HEK293 cells expressing the constructs used throughout the manuscript for fluorescence microscopy. Clockwise, SNAP-β1AR, SNAP-MC4R, SNAP-MC4R in presence of MRAP2 (1+4), SNAP-MC4RChim, examples of eYFP-MRAP2 and finally SNAP-CXCR4. All labeled with SNAP-surface Alexa 647. **(B)** Molecular brightness values of SNAP-β1AR and SNAP-CXCR4 labeled with SNAP-surface Alexa 647, used respectively as monomeric and dimeric control. **(C)** Snake plot diagram illustrating the mutated residues in ICL2 loops to generate MC4Rchim.

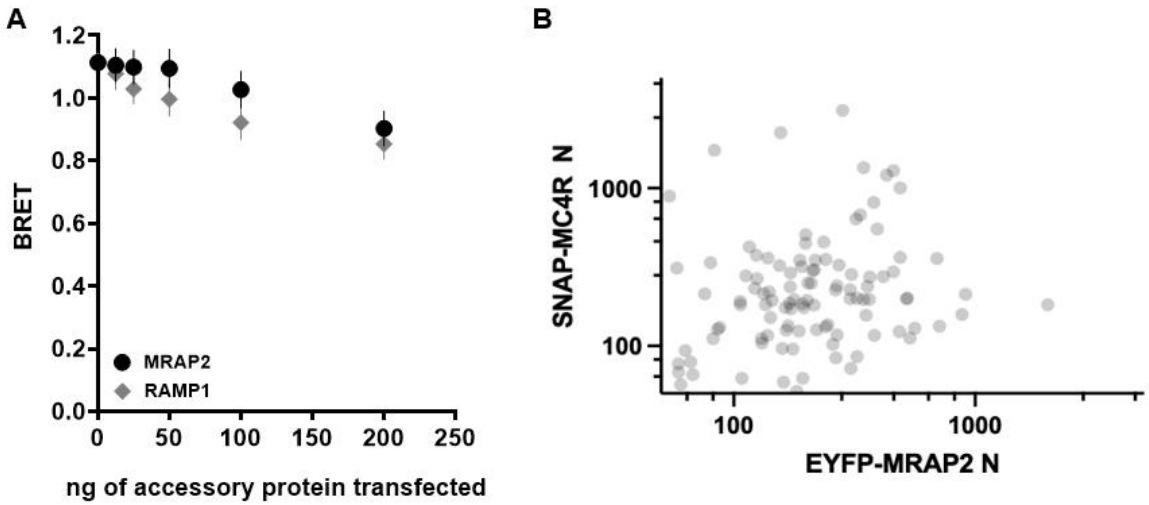

Supplementary Figure 7: Dependence of MC4R surface expression of MRAP2 expression levels. (A) BRET readout of the abundance of MC4R-RlucII at the plasma membrane based on bystander BRET levels with the acceptor rGFP-CAAX in the presence or absence of increasing amount of MRAP2 or RAMP1 in transiently transfected HEK293-SL cells. Total DNA is fixed. Data are expressed as mean ± SEM of three independent experiments. **(B)** Scatter plot illustrating the relationship between the number of SNAP-MC4Rs at the plasma membrane and eYFP-MRAP2 expression. Data were extracted from spatial brightness analysis of confocal micrographs as those display in Supplementary Figure 5A.

```
hMRAP1   . . . . . . . M A N G T N A S A P Y Y S Y E Y Y L D Y L D L I P V D E K K L K A   33
hMRAP2   M S A Q R L I S N R T S Q Q S A S N S D Y T W E Y E Y Y E I G P V S F E G L K A   40

hMRAP1   H K H S I V I A F W V S L A A F V V L L F L I L L Y M S W S A S P Q M R N S P K   73
hMRAP2   H K Y S I V I G F W V G L A V F V I F M F F V L T L L T K T G A P H Q D N A E S   80

hMRAP1   H H Q T C P W S H G L N L H L C I Q K C L P C H R E P L A T S Q A Q A S S V E P   113
hMRAP2   S E K R F R M N S F V S D F G R P L E P D K V F S R Q G N E E S R S L F H C Y I   120

hMRAP1   G S R T G P D Q P L R Q E S S S T L P L G G F Q T H P T L L W E L T L N G G P L   153
hMRAP2   N E V E R L D R A K A C H Q T T A L D S D V Q L Q E A I R S S G Q P E E E L N R   160

hMRAP1   V R S K P S E P P P G D R T S Q L Q S . . . . . . . . . . . . . . . . . . . .   172
hMRAP2   L M K F D I P N F V N T D Q N Y F G E D D L L I S E P P I V L E T K P L S Q T S   200

hMRAP1   . . . . .   172
hMRAP2   H K D L D   205
```

Supplementary Figure 8: Alignment of the human MRAP1 and MRAP2 sequences. Alignment was visualized using the software BioEdit [Hall, T.A. BioEdit: a user-friendly biological sequence alignment editor and analysis program for Windows 95/98/NT. . Nucl. Acids. Symp. Ser. 1999; 41: 95-98]. Specific background colors reflecting physicochemical properties of the amino acid side chains: black - proline; blue - positively charged; cyan/green - aromatic and hydrophobic; green - hydrophobic; red - negatively charged; grey - hydrophilic; dark red - cysteines; and magenta – histidine

METHODS

Cell culture

Different variants of Human Embryonic Kidney cells (HEK293) were employed. HEK293T cell line (ECACC 96121229, Sigma-Aldrich) was used for plater reader and receptor localization and trafficking experiments. HEK293Adherent (HEK293AD) cell line (R70507, Thermo Fisher) was used for molecular brightness experiments (SpIDA). We refer to all three clones of HEK293 cells as HEK293 in the main text. Cells were grown in Dulbecco's Modified Eagle's Medium (DMEM, Pan Biotech), supplemented with 2 mM L-glutamine (Pan Biotech), 10 % (v:v) heat-inactivated Fetal Calf Serum (Biochrome), 100 µg/mL streptomycin, and 100 U/mL penicillin (Gibco) at 37 °C in a 5 % CO_2 incubator. HEK293 cells were grown in T75 cm^2 flasks. Upon reaching approximately 80 % confluency, cells were washed with 5 mL phosphate-buffered saline without Ca^{2+} and Mg^{2+} ions (DPBS, Sigma-Aldrich), trypsinised using 3 mL 0.05 % / 0.02 % trypsin/ethylenediaminetetraacetic acid solution (Pan Biotech) and passaged every 2 to 3 days. Cells were routinely tested for mycoplasma infection using MycoAlert Mycoplasma Detection Kit (Lonza).

Seeding and transfection

25-mm glass coverslips and 96-well microtiter plates were coated with poly-D-lysine (PDL) (1 mg/ml) for 30 minutes, washed twice with PBS, and left to dry before seeding. For microscopy experiments, 3×10^5 cells were seeded on to clean and PDL-coated glass coverslips (Sigma-Aldrich) into a six-well plate, whereas cell seeding density of 40,000 cells per well was used for plate reader assays. After 24 h, cells were transfected with JetPrime, according to the manufacturer's protocol. For all transfections, MC4R:pcDNA3/MRAP2 ratio was 1:4, unless otherwise noted. The empty backbone of pcDNA3 as mock was used throughout to maintain a consistent level of total cDNA. Plasmid DNA constructs for hMC4R, MC4RChim and hMRAP2 were kindly provided by Prof. Heike Biebermann (Charite) and subcloned into pcDNA3 and pVITRO2 backbones using Gibson assembly with appropriate SNAP- and eYFP tags respectively.

Transfection via Lipofectamine 3000

HEK293 cells were transiently transfected following the reverse transfection method using Lipofectamine™ 3000 (Thermo Fisher). Two transfection mixes (A & B) were prepared, in Mix A the DNA was diluted in 25 mL OptiMEM® media, and in Mix B 0.3 mL/well of P3000™ was added. In Mix B, 0.3 mL/well of Lipofectamine™ was added to 25 mL OptiMEM® media and each mix was incubated for 5 min. The DMEM in the HEK293 cells at approximately 70 % to 85 % confluency was removed and washed with DPBS without Ca^{2+} and Mg^{2+}, trypsinised and centrifuged as described above. Meanwhile, Mix A containing the DNA was added to Mix B containing Lipofectamine™ mix dropwise and incubated for 15 min at room temperature. The cell pellet was resuspended in 10 mL DMEM-High Glucose media, counted and diluted at a density of 75,000 cells/well. 50 µL of the transfection mix was added into a poly-D-lysine (Sigma-Aldrich) coated clear white F-bottom 96-well plate followed by 100 mL of the cell suspension. The plate was incubated at 37 °C in a 5 % CO_2 incubator for 24 h.

FRET-sensor based cAMP assay

HEK293T cells were seeded into 10 cm Petri dishes ($3.5x10^6$ cells) and after 24 h transfected with the combination of Epac-S^{H187} FRET biosensor, pcDNA3, SNAP-MC4R and Epac-S^{H187} biosensor, SNAP-MC4R and MRAP2. Plasmid DNA combinations were transfected at a ratio of 5:1:1 or 5:1:4 respectively. Media was changed 4 h after transfection. Twenty-four hours post-transfection, cells were re-seeded into PDL-coated black-wall, black bottom 96-well plates at a density of 40,000 cells per well. 36 h after transfection, cells were washed, and medium was changed to HBSS buffer supplemented with 0.1 % BSA. Plate reader experiments were performed using a Synergy Neo2 plate reader (BioTek) equipped with a monochromator and filter optics. Expression levels of receptor, biosensor and accessory protein were measured with monochromator optics. For expression of MC4R and MRAP2, cells were excited at 558/20 nm and fluorescence emission was recorded at 605/20 nm while for biosensor the excitation was at 500/20 nm, and emission was at 539/20 nm. For FRET measurements, a range of CFP/YFP monochromators were used, which was excited at 430/20 nm, while 491/30 nm and 541/20 nm were used for emission.

In 90 µL HBSS buffer, acceptor baseline fluorescence was measured. Then, pre-stimulation basal reads for 5 minutes were recorded. Afterwards, 10 µL of 10-fold ligand solution was applied to each well and the post-stimulation reads were recorded for a further 25 min. Subsequently, Forskolin/IBMX was added to each well to record maximal stimulation reads.

cAMP signaling assay with Glo sensor

The transfection mix was prepared, in Mix A, 50 ng/well of pGloSensor™-22F cAMP sensor plasmid (Promega), 50 ng/well of the 3x HA MC4R plasmid and 50 ng/well pcDNA3.1 or MRAP2-FLAG were added to 25 mL/well OptiMEM® media. To this, 0.3 mL/well of P3000™ was added. In Mix B, 0.3 mL/well of Lipofectamine™ was added to 25 mL OptiMEM®. 24 h after transfection via lipofectamine, the cell culture media was removed and the cells were washed with cAMP assay buffer (1x HBSS, 24 mM HEPES, 0.1 % (*w:v*) BSA, 3.96 mM $NaHCO_3$, 1 mM $MgSO_4$, 1.3 mM $CaCl_2$ ($2H_2O$), pH 7.4). The plate was then equilibrated for 1 hour at 28 °C with 70-90 mL of cAMP buffer supplemented with 0.45 mg/mL of Firefly D-Luciferin free acid (NanoLight Technology). If Dynasore (HelloBio) is incorporated into the experiment an additional step is taken, whereby post equilibration, 20 µL of Dynasore (80 µM/well) is added to each well and incubated for 15 min at room temperature. Thereafter, the basal readings are performed on the CLARIOstar® Plus Plate Reader (BMG LabTech, Germany) and the relative luminescence units (RLU) were measured for approximately 5 minutes before stimulating the cells with 10 µL of agonist, vehicle or forskolin. The final volume in each well was 100 µL. An average of the basal reads was used to normalize the response of each well. Bioluminescence was measured for a total of 66 cycles (1 min per cycle), with a 1-second integration time and no lens.

Nanobody recruitment assay

HEK293AD cells were seeded in PDL-coated 8-well Ibidi slides at a density of 25000 cells per well, following with JetPrime transfection the next day, according to the manufacturer's protocol. Plasmid DNA ratios used for co-transfection were as follows: for Nb35/37 recruitment, 1x SNAP-MC4R+4x pcDNAmock/MRAP2, 1x Nb35-eYFP/Nb37-eYFP and 3x Gs (tricistronic). Next day, transfected cells were labeled with SNAP-Surface Alexa Fluor 647 dye (NEB) as described earlier. Afterwards, cells were subsequently taken for imaging to an Attofluor Cell Chamber (Fisher Scientific, GmbH) in 1x HBSS supplemented with 0.1 % BSA. A TIRF illuminated Eclipse Ti2 microscope (Nikon), equipped with a 100X, 1.49 NA automated correction collar objective, and with 405, 488, 561, and 647 nm laser diodes coupled via an automated N-Storm module and four iXon Ultra 897 EMCCD cameras (Andor), was used. During imaging, both the cell imaging chamber holding Ibidi slide, and objectives were kept at 37 °C. The automated objective collar was kept on and hardware autofocus was activated. The acquisition of movies was performed at 4 seconds per frame for 400 frames. Initially, a baseline measurement of 25 frames was done and then NDP-α-MSH was added at a concentration of 1 µM to the well. Fluorescence intensity values were extracted by employing ImageJ. Background correction and normalization was made for pre-stimulation and post-stimulation.

IP_1 accumulation assay

Cellular IP1 as a readout for Gq signaling was measured using a commercial HTRF competitive immunoassay (IP-One Gq kit, CisBio) as described in the manufacturer's protocol. For this purpose, HEK293T cells were seeded into 10 cm Petri dishes ($3.5x10^6$ cells) and after 24 h transfected with the combination of plasmids (pcDNA3+SNAP-MC4R) and (SNAP-MC4R+MRAP2) at a ratio of 1:4, using JetPrime according to the manufacturer's protocol. Media was changed 4 h after transfection. Twenty-four hours post-transfection, 20 µL of cell suspension at a density of 15,000 cells per well was re-seeded into opaque white flat-bottom 384-well plates (Corning) and left to equilibrate for 2 hours at 37 °C in a 5 % CO2 incubator. Afterwards, the cells were stimulated with ligand concentrations (dilution series for concentration response curve) prepared in stimulation buffer (HBSS supplemented with 20mM LiCl) for 2 hours under cell culture conditions. Following incubation, the FRET acceptor (IP_1-d2) and the FRET donor (anti-IP_1-Cryptate antibody) were reconstituted and diluted in lysis and detection buffer as described in the manufacturer's protocol. 3 µL each of both solutions was added per well separately in the order described, and the plate was incubated on a shaker for an hour at room temperature. Fluorescence emission was detected at 620 nm and 665 nm at the plate reader (Synergy Neo2 plate reader, BioTek). The HTRF ratio was calculated by dividing the detected emission at 665 nm by the detected emission at 620 nm. The EC_{50} values were calculated using the GraphPad Prism 10 software (GraphPad Software, San Diego, CA, USA).

NFAT reporter assay

HEK293 cells were transfected 24 hours after seeding. For determination of phospholipase C (PLC) activation (read-out for Gq/11 signaling) via nuclear factor of activated T-cells (NFAT) reporter gene assay, cells were transfected with 45 ng plasmid-DNA, 0.45 µl Metafectene (Biontex, Munich, Germany) and with 45 ng NFAT reporter DNA per well in MEM without supplements.

For PLC activation, the NFAT responsive element (NFAT-luc, pGL4.33) was co-transfected with the plasmids for MC4R and MRAP2 in a ratio of 1+1 (1:1) or 1+4 (1:4). 48h post transfection, cells were challenged with α-MSH (10 mM to 1 nM) in MEM without supplements for 4 h at 37 °C and 5 % CO_2. The stimulation was stopped by discarding the media and cell lysis was induced by addition of 1x passive lysis buffer (PLB, Promega) and horizontal shaking for 15 min at room temperature.

For measurement of luciferase activity, 10 µl lysate were transferred into a white opaque 96 well plate. Injection of 40 µl firefly luciferase substrate (Promega) and measurement of luminescence was performed with a plate reader (Viktor Nivo, Perkin Elmer).

SNAP Tag labeling

Prior to microscopy imaging experiments, coverslips with cells expressing SNAP-MC4R and MRAP2 were labeled with 1 µM SNAP-Surface Alexa Fluor 647 dye in complete DMEM (Pan Biotech) for 25 min and kept in the incubator at 37 °C and 5 % CO_2. Excessive dye was washed by exchanging with fresh medium with an interval of 5 minutes each for three times.

Time-lapse imaging with confocal microscopy

HEK293T cells ($3x10^5$ cell per well) were seeded on 25 mm glass coverslips in a 6-well plate, which were pre-coated with PDL. After 24 hours, cells were transfected with 2.5 µg DNA in total of SNAP-MC4R and MRAP2 constructs (1:4 ratio) using JetPrime according to the manufacturer's protocol. Media was exchanged to fresh media 4 hours after transfection. Next day, transfected cells were labeled with SNAP-Surface Alexa Fluor 647 dye. Afterwards, coverslip with labeled cells was placed in the Attofluor cell chamber (Thermo Fisher Scientific) with 450 µL of the imaging buffer (HBSS supplemented with 0.1 % BSA) and the chamber was placed in the placeholder for image acquisition. Pre-stimulation images were taken for the first 3-5 minutes and then 50 µL of agonist NDP-α-MSH was carefully added on top of cells to the final concentration of 1µM in the chamber and image acquisition was performed for 30 min post-stimulation.

Imaging was performed using Leica SP8 confocal microscope system with 40x/1.25 NA oil immersion objective, a photon counting hybrid detectors and a white light laser (WLL). 488 and 633 nm lines of the WLL were used for excitation and emission bands of 520 nm to 600 nm and 650 nm to 730 nm were used for detection of eYFP and SNAP-Surface Alexa 647, respectively. Imaging format was xyt, and image size was set to 1024×1024 pixels and 100 Hz scan speed. Image analysis was performed using ImageJ.

NanoBiT arrestin recruitment assay

HEK293 cells (75,000 cells/well) were seeded in white bottom 96-well plate and reverse co-transfected with Lipofectamine 3000, whereby the plasmid encoding the MC4R-LgBiT (50 ng/well) and the SmBiT-β-arrestin 2 (10 ng/well) were used. 24 h post-transfection, the cells were rinsed once with assay buffer (1X HBSS, 24 mM HEPES, 0.1% (*w:v*) BSA, 3.96 mM $NaHCO_3$, 1 mM $MgSO_4$, 1.3 mM $CaCl_2$ ($2H_2O$), pH 7.4) and the plates were pre-equilibrated in the dark for 1h at 37 °C with 90 µL of assay buffer. Post-equilibration, 25 µL/well of a 5x solution of the Nano-Glo® Live cell reagent (NanoLight Technology) was added, and luminescence readings were taken every minute at 37 °C until the signal was stable (3-5 min), representing the basal activity. Immediately after, 10 µL of agonist/vehicle were added and luminescence was further recorded for 60 min (no lens, 0.5 s integration time and 1 min intervals at 37 °C using a CLARIOstar® Plus Multimode Plate Reader (BMG Labtech, Germany). The final volume in each well was 125 µL. To account for differences in expression/cell density, the average of at least 3 stable pre-readings was used to normalize each well response before proceeding with further analysis using the area under the curve parameter.

Molecular brightness analysis with SpIDA

HEK293AD cells (3×10^5 cells/well) were seeded on clean glass coverslips in six-well plates and were transfected with MC4R and MRAP2 constructs for overnight using JetPrime as a transfection reagent according to the manufacturer's protocol. For SNAP-tag incorporated receptors, labeling was performed as described above using SNAP-Surface Alexa Fluor 647 dye. Coverslips with transfected cells were placed in an Attofluor cell chamber (Thermo Fisher Scientific) and supplemented with Flourobrite DMEM supplemented with 2 mM L-glutamine (Pan Biotech), 10% fetal calf serum (Biochrome), 100 µg/mL streptomycin, and 100 U/mL penicillin (Gibco). SpIDA imaging was performed using a commercial laser-scanning confocal microscope (Leica SP8) equipped with a 40×/1.25 NA oil immersion objective, a white light laser (WLL), and photon counting hybrid detectors; 514 and 633 nm lines of the WLL were used for excitation, and emission bands of 520 nm to 600 nm and 650 nm to 730 nm were used for detection of eYFP and SNAP-Surface Alexa 647, respectively. Imaging format was xy, and image size was set to 512 × 512 pixels with 50 nm pixel size and 100Hz scan speed. Image analysis was performed using ImageJ. Polygonal region of interest (ROI) selection was implemented and areas with inhomogeneous fluorescence distribution were avoided.

Homology modeling of MC4R–MRAP2 complex

A structural homology model of an agonist–MC4R–MRAP2–Gs complex was designed based on the recently determined ACTH–MC2R–MRAP1–Gs complex (PDB ID: 8GY7)[15] and the NDP-α-MSH–MC4R–Gs protein complex (PDB ID: 7PIV)[36] as structural templates. Both complexes were superimposed at the receptor transmembrane region, and MRAP was merged from the ACTH–MC2R–MRAP1–Gs complex into the NDP-α-MSH–MC4R–Gs protein complex. NDP-α-MSH was substituted by α-MSH as known from the α-MSH–MC4R complex[62]. The sequence of MRAP1 was substituted by corresponding amino acid residues of MRAP2. For all steps the software SYBYL-X 2.0 (Certara, NJ, US) was used and the initial complex model was optimized by energy minimization with the Amber99 force field until converging at a termination gradient of 0.05 kcal/(mol*Å) under constrained backbone atoms. Side chain orientations were optimized by a 2 ns molecular dynamics simulation (MD) with constraint backbone atoms. Finally, the entire complex model α-MSH–MC4R–MRAP2–Gs was energetically minimized without any constraint.

BRET-based assays

HEK293-SL cells[42], a subclone of Ad5-transformed HEK293 cells kindly given by S. Laporte (McGill University, Montreal, Canada), were cultured in DMEM (Wisent Bioproducts) supplemented with 10% newborn calf serum (Wisent Bioproducts) and 100 UI/mL penicillin and 100 µg/mL streptomycin (Wisent Bioproducts) in an incubator set to 37°C and 5% CO_2. Cells were routinely tested for mycoplasma infection using PCR Mycoplasma Detection Kit (ABM#G238).

The day of the transfection, cells are distributed 100 uL per well at a density of 350,000 cells/mL in Cellstar© opaque white 96-well plates (Greiner Bio-One) with 1 µg/mL of total plasmid DNA and 3 µg/mL of 25 kDA linear polyethyleneimine (Alfa Aesar). Plasmids encoding for Rluc8-C1_Rluc8-miniGs[38], pcDNA3.1hygro(+)_p63RhoGEF-RlucII, pcDNA3.1hygro(+)_Rap1GAP-RlucII[39], pcDNA3.1hygro(+)_β-arrestin2-RlucII, pcDNA3.1(+)_rGFP-CAAX, pcDNA3.1(+)_rGFP-FYVE, and pcDNA3.1(+)_MRAP2 were already described[42,63,64]. RAMP1 and RAMP3 were kindly provided by S. M. Foord (GlaxoSmithKline) and subcloned into pcDNA3 as previously described. pcDNA3.1_$G\alpha_q$ and pcDNA3.1_$G\alpha_{15}$ were purchased from cDNA Resource Center. New pcDNA.3.1(+)_MC4R-RlucII was generated from 3xHA-hMC4R-RlucII using Gibson assembly to remove the N-terminal 3xHA tag and to add a full Kozak consensus sequence before the receptor, and to replace the linker with GGGGSKLPAT between the human MC4R (MCR040TN00, cDNA Ressource Center) and the RlucII[42]. For the BRET assays, the SNAP-MC4R is in a pVITRO2 dual expression vector (Invivogen), in which mRuby2 is expressed under the FerL promoter, and the MC4R is expressed under the FerH promoter. The MC4R is N-terminally tagged with consecutively an Ig kappa ladder signal peptide (Igκ), a hemagglutinin A (HA) tag, a Strep-Tag®II (ST) tag and a SNAP-tag® (Igκ-HA-ST-SNAP-MC4R).

Total plasmid transfected was adjusted to 1000 ng with pcDNA3.1(+) and fixed plasmid amounts were as follows: 25 ng MC4R-RlucII, 400 ng rGFP-FYVE, 300 ng rGFP-CAAX, 5 ng p63RhoGEF-RlucII with 100 ng $G\alpha_q$, 10 ng p63RhoGEF with 50 ng $G\alpha_{15}$, 5 ng β-arrestin2-RlucII, 5 ng Rluc8-miniGs. Polyscistronic pVITRO_SNAP-MC4R amounts were adjusted to be around the middle of the linear range of each functional assays, which is 100 ng for miniGs recruitment assay, 140 ng for β-arrestin recruitment assay, 400 ng for p63RhoGEF recruitment assay with $G\alpha_q$, 10 ng for p63RhoGEF recruitment assay with $G\alpha_{15}$. MRAP2 amounts were used at varying amounts, but RAMP3 amounts were only tested at the higher of the MC4R:MRAP2 ratio used.

Two days after transfection, plates were washed with PBS supplemented with 1 mM $CaCl_2$ and 1 mM $MgCl_2$, and equilibrated at 37°C for approximately 1h in Tyrode HEPES buffer (NaCl 137 mM, $MgCl_2$ 1 mM, $NaHCO_3$ 11.9 mM, NaH_2PO_4 3.6 mM, KCl 0.9 mM, glucose 5.5 mM, $CaCl_2$ 1 mM, with pH adjusted to 7.4 with NaOH). Total fluorescence of the rGFP ($\lambda_{excitation}$ 485 nm, $\lambda_{emission}$ 538 nm, auto cutoff 530 nm) and/or the mRuby2 ($\lambda_{excitation}$ 550 nm, $\lambda_{emission}$ 615 nm, cutoff set to 610 nm) was red before BRET experiments using FLEX station II (Molecular Devices), respectively to control for plasmid competition of the biosensors and dual expression of the pVITRO2_MC4R.

For dose-response curve experiments, cells were incubated with increasing concentrations of α-MSH (GenScript) with 0.01% m/V bovine serum albumin (Biobasic) for 45 minutes for G protein activation assays, for 2 or 3 minutes for β-arrestin2 recruitment assay and for 60 minutes for internalization assay. Prolume Purple methoxy e-Coelenterazine (NanoLight Technology) was added 10 minutes before reading (1 µM final). Light measurements at 410/80 nm (donor) and 515/20 nm (acceptor) channels were integrated for 0.1 second at 37°C on Tristar² LB942 (Berthold Technology). BRET is calculated as the ratio of the light emitted in the acceptor channel over the light emitted in the donor channel.

Results were normalized to the α-MSH-induced change in BRET ratio of the mock condition.

$$\alpha\text{-MSH-induced change in BRET (\%)} = \frac{\text{BRET}_{\text{condition}} - \text{bottom asymptote}_{\text{condition}}}{\text{span}_{\text{mock}}} * 100$$

Concentration-response curves and parameters, such as bottom asymptote, span and $\log EC_{50}$ were calculated by GraphPad Prism using 3-parameters non-linear regression. E_{max} is calculated manually as span ratio over the mock. It is to note that all calculations excluded changes in basal.

$$E_{max}\ (\%) = \frac{\text{span}_{\text{condition}}}{\text{span}_{\text{mock}}} * 100$$

Statistical analysis were performed on GraphPad Prism (10.2.1) using ordinary one-way ANOVA with Dunnett's multiple comparisons post-hoc test.

REFERENCES

1 Wang, M. *et al.* Identification of MRAP protein family as broad-spectrum GPCR modulators. *Clin Transl Med* **12**, e1091, doi:10.1002/ctm2.1091 (2022).

2 Rouault, A. A. J., Lee, A. A. & Sebag, J. A. Regions of MRAP2 required for the inhibition of orexin and prokineticin receptor signaling. *Biochim Biophys Acta Mol Cell Res* **1864**, 2322-2329, doi:10.1016/j.bbamcr.2017.09.008 (2017).

3 Lattanzi, R. *et al.* MRAP2 Inhibits beta-Arrestin-2 Recruitment to the Prokineticin Receptor 2. *Curr Issues Mol Biol* **46**, 1607-1620, doi:10.3390/cimb46020104 (2024).

4 Asai, M. *et al.* Loss of function of the melanocortin 2 receptor accessory protein 2 is associated with mammalian obesity. *Science* **341**, 275-278, doi:10.1126/science.1233000 (2013).

5 Klein, K. R., Matson, B. C. & Caron, K. M. The expanding repertoire of receptor activity modifying protein (RAMP) function. *Crit Rev Biochem Mol Biol* **51**, 65-71, doi:10.3109/10409238.2015.1128875 (2016).

6 Serafin, D. S., Harris, N. R., Nielsen, N. R., Mackie, D. I. & Caron, K. M. Dawn of a New RAMPage. *Trends Pharmacol Sci* **41**, 249-265, doi:10.1016/j.tips.2020.01.009 (2020).

7 Mainland, J. & Matsunami, H. RAMP like proteins : RTP and REEP family of proteins. *Adv Exp Med Biol* **744**, 75-86, doi:10.1007/978-1-4614-2364-5_7 (2012).

8 Fan, S., Liu, H. & Li, L. The REEP family of proteins: Molecular targets and role in pathophysiology. *Pharmacol Res* **185**, 106477, doi:10.1016/j.phrs.2022.106477 (2022).

9 Peters, C. H., Singh, R. K., Bankston, J. R. & Proenza, C. Regulation of HCN Channels by Protein Interactions. *Front Physiol* **13**, 928507, doi:10.3389/fphys.2022.928507 (2022).

10 McLatchie, L. M. *et al.* RAMPs regulate the transport and ligand specificity of the calcitonin-receptor-like receptor. *Nature* **393**, 333-339, doi:10.1038/30666 (1998).

11 Hay, D. L., Poyner, D. R. & Sexton, P. M. GPCR modulation by RAMPs. *Pharmacol Ther* **109**, 173-197, doi:10.1016/j.pharmthera.2005.06.015 (2006).

12 Chan, L. F. *et al.* MRAP and MRAP2 are bidirectional regulators of the melanocortin receptor family. *Proc Natl Acad Sci U S A* **106**, 6146-6151, doi:10.1073/pnas.0809918106 (2009).

13 Webb, T. R. & Clark, A. J. Minireview: the melanocortin 2 receptor accessory proteins. *Mol Endocrinol* **24**, 475-484, doi:10.1210/me.2009-0283 (2010).

14 Metherell, L. A. *et al.* Mutations in MRAP, encoding a new interacting partner of the ACTH receptor, cause familial glucocorticoid deficiency type 2. *Nat Genet* **37**, 166-170, doi:10.1038/ng1501 (2005).

15 Luo, P. *et al.* Structural basis of signaling regulation of the human melanocortin-2 receptor by MRAP1. *Cell Res.* **33**, 46-54, doi:10.1038/s41422-022-00751-6 (2023).

16 Sebag, J. A. & Hinkle, P. M. Melanocortin-2 receptor accessory protein MRAP forms antiparallel homodimers. *Proc Natl Acad Sci U S A* **104**, 20244-20249, doi:10.1073/pnas.0708916105 (2007).

17 Hofland, J. *et al.* Melanocortin 2 receptor-associated protein (MRAP) and MRAP2 in human adrenocortical tissues: regulation of expression and association with ACTH responsiveness. *J Clin Endocrinol Metab* **97**, E747-754, doi:10.1210/jc.2011-2328 (2012).

18 Bruschetta, G., Kim, J. D., Diano, S. & Chan, L. F. Overexpression of melanocortin 2 receptor accessory protein 2 (MRAP2) in adult paraventricular MC4R neurons regulates energy intake and expenditure. *Molecular metabolism* **18**, 79-87, doi:10.1016/j.molmet.2018.09.010 (2018).

19 Liang, J. *et al.* Pharmacological effect of human melanocortin-2 receptor accessory protein 2 variants on hypothalamic melanocortin receptors. *Endocrine* **61**, 94-104, doi:10.1007/s12020-018-1596-2 (2018).

20 Bernard, A. *et al.* MRAP2 regulates energy homeostasis by promoting primary cilia localization of MC4R. *JCI Insight* **8**, doi:10.1172/jci.insight.155900 (2023).

21 Kuhnen, P., Krude, H. & Biebermann, H. Melanocortin-4 Receptor Signalling: Importance for Weight Regulation and Obesity Treatment. *Trends Mol Med* **25**, 136-148, doi:10.1016/j.molmed.2018.12.002 (2019).

22 Clement, K. *et al.* MC4R agonism promotes durable weight loss in patients with leptin receptor deficiency. *Nat Med* **24**, 551-555, doi:10.1038/s41591-018-0015-9 (2018).

23 Heyder, N. *et al.* Signal Transduction and Pathogenic Modifications at the Melanocortin-4 Receptor: A Structural Perspective. *Front. Endocrinol. (Lausanne)* **10**, 515, doi:10.3389/fendo.2019.00515 (2019).

24 Baron, M. *et al.* Loss-of-function mutations in MRAP2 are pathogenic in hyperphagic obesity with hyperglycemia and hypertension. *Nat. Med.* **25**, 1733-1738, doi:10.1038/s41591-019-0622-0 (2019).

25 Cai, Z., Christensen, O. F., Lund, M. S., Ostersen, T. & Sahana, G. Large-scale association study on daily weight gain in pigs reveals overlap of genetic factors for growth in humans. *BMC Genomics* **23**, 133, doi:10.1186/s12864-022-08373-3 (2022).

26 Sebag, J. A., Zhang, C., Hinkle, P. M., Bradshaw, A. M. & Cone, R. D. Developmental control of the melanocortin-4 receptor by MRAP2 proteins in zebrafish. *Science* **341**, 278-281, doi:10.1126/science.1232995 (2013).

27 Li, Y. Q. *et al.* G(q/11)alpha and G(s)alpha mediate distinct physiological responses to central melanocortins. *J. Clin. Invest.* **126**, 40-49, doi:10.1172/JCI76348 (2016).

28 Schonnop, L. *et al.* Decreased melanocortin-4 receptor function conferred by an infrequent variant at the human melanocortin receptor accessory protein 2 gene. *Obesity (Silver Spring)* **24**, 1976-1982, doi:10.1002/oby.21576 (2016).

29 Reininghaus, N. *et al.* A Setmelanotide-like Effect at MC4R Is Achieved by MC4R Dimer Separation. *Biomolecules* **12**, doi:10.3390/biom12081119 (2022).

30 Brouwers, B. *et al.* Human MC4R variants affect endocytosis, trafficking and dimerization revealing multiple cellular mechanisms involved in weight regulation. *Cell Rep* **34**, 108862, doi:10.1016/j.celrep.2021.108862 (2021).

31 Piechowski, C. L. *et al.* Inhibition of melanocortin-4 receptor dimerization by substitutions in intracellular loop 2. *J. Mol. Endocrinol.* **51**, 109-118, doi:10.1530/jme-13-0061 (2013).

32 Elsner, A. *et al.* MC4R oligomerizes independently of extracellular cysteine residues. *Peptides* **27**, 372-379, doi:10.1016/j.peptides.2005.02.027 (2006).

33 Scarselli, M. *et al.* Revealing G-protein-coupled receptor oligomerization at the single-molecule level through a nanoscopic lens: methods, dynamics and biological function. *FEBS J* **283**, 1197-1217, doi:10.1111/febs.13577 (2016).

34 Klarenbeek, J., Goedhart, J., van Batenburg, A., Groenewald, D. & Jalink, K. Fourth-generation epac-based FRET sensors for cAMP feature exceptional brightness, photostability and dynamic range: characterization of dedicated sensors for FLIM, for ratiometry and with high affinity. *PLoS One* **10**, e0122513, doi:10.1371/journal.pone.0122513 (2015).

35 Rasmussen, S. G. *et al.* Crystal structure of the beta2 adrenergic receptor-Gs protein complex. *Nature* **477**, 549-555, doi:10.1038/nature10361 (2011).

36 Heyder, N. A. *et al.* Structures of active melanocortin-4 receptor-Gs-protein complexes with NDP-alpha-MSH and setmelanotide. *Cell Res.* **31**, 1176-1189, doi:10.1038/s41422-021-00569-8 (2021).

37 Sawyer, T. K. *et al.* 4-Norleucine, 7-D-phenylalanine-alpha-melanocyte-stimulating hormone: a highly potent alpha-melanotropin with ultralong biological activity. *Proc Natl Acad Sci U S A* **77**, 5754-5758, doi:10.1073/pnas.77.10.5754 (1980).

38 Wright, S. C. *et al.* GLP-1R signaling neighborhoods associate with the susceptibility to adverse drug reactions of incretin mimetics. *Nat Commun* **14**, 6243, doi:10.1038/s41467-023-41893-4 (2023).

39 Avet, C. *et al.* Effector membrane translocation biosensors reveal G protein and betaarrestin coupling profiles of 100 therapeutically relevant GPCRs. *eLife* **11**, doi:10.7554/eLife.74101 (2022).

40 Grundmann, M. & Kostenis, E. Temporal Bias: Time-Encoded Dynamic GPCR Signaling. *Trends Pharmacol Sci* **38**, 1110-1124, doi:10.1016/j.tips.2017.09.004 (2017).

41 Ollmann, M. M. *et al.* Antagonism of central melanocortin receptors in vitro and in vivo by agouti-related protein. *Science* **278**, 135-138 (1997).

42 Namkung, Y. *et al.* Monitoring G protein-coupled receptor and beta-arrestin trafficking in live cells using enhanced bystander BRET. *Nat Commun* **7**, 12178, doi:10.1038/ncomms12178 (2016).

43 Janetzko, J. *et al.* Membrane phosphoinositides regulate GPCR-beta-arrestin complex assembly and dynamics. *Cell* **185**, 4560-4573 e4519, doi:10.1016/j.cell.2022.10.018 (2022).

44 Isbilir, A. *et al.* Advanced fluorescence microscopy reveals disruption of dynamic CXCR4 dimerization by subpocket-specific inverse agonists. *Proc Natl Acad Sci U S A* **117**, 29144-29154, doi:10.1073/pnas.2013319117 (2020).

45 Isbilir, A. *et al.* Determination of G-protein-coupled receptor oligomerization by molecular brightness analyses in single cells. *Nat. Protoc.* **16**, 1419-1451, doi:10.1038/s41596-020-00458-1 (2021).

46 Ward, R. J. *et al.* Chemokine receptor CXCR4 oligomerization is disrupted selectively by the antagonist ligand IT1t. *J Biol Chem* **296**, 100139, doi:10.1074/jbc.RA120.016612 (2021).

47 Kay, E. I., Botha, R., Montgomery, J. M. & Mountjoy, K. G. hMRAPa increases alphaMSH-induced hMC1R and hMC3R functional coupling and hMC4R constitutive activity. *J Mol Endocrinol* **50**, 203-215, doi:10.1530/JME-12-0221 (2013).

48 Soletto, L. *et al.* Melanocortin Receptor Accessory Protein 2-Induced Adrenocorticotropic Hormone Response of Human Melanocortin 4 Receptor. *J Endocr Soc* **3**, 314-323, doi:10.1210/js.2018-00370 (2019).

49 Wu, B. *et al.* Structures of the CXCR4 chemokine GPCR with small-molecule and cyclic peptide antagonists. *Science* **330**, 1066-1071, doi:10.1126/science.1194396 (2010).

50 Manglik, A. *et al.* Crystal structure of the micro-opioid receptor bound to a morphinan antagonist. *Nature* **485**, 321-326, doi:10.1038/nature10954 (2012).

51 Metzger, P. J. *et al.* A human obesity-associated MC4R mutation with defective Gq/11alpha signaling leads to hyperphagia in mice. *J Clin Invest* **134**, doi:10.1172/JCI165418 (2024).

52 Buch, T. R., Heling, D., Damm, E., Gudermann, T. & Breit, A. Pertussis toxin-sensitive signaling of melanocortin-4 receptors in hypothalamic GT1-7 cells defines agouti-related protein as a biased agonist. *J. Biol. Chem.* **284**, 26411-26420, doi:10.1074/jbc.M109.039339 (2009).

53 Angers, S. *et al.* Detection of beta 2-adrenergic receptor dimerization in living cells using bioluminescence resonance energy transfer (BRET). *Proc Natl Acad Sci U S A* **97**, 3684-3689, doi:10.1073/pnas.97.7.3684 (2000).

54 Hebert, T. E. *et al.* A peptide derived from a beta2-adrenergic receptor transmembrane domain inhibits both receptor dimerization and activation. *J Biol Chem* **271**, 16384-16392, doi:10.1074/jbc.271.27.16384 (1996).

55 Paradis, J. S. *et al.* Computationally designed GPCR quaternary structures bias signaling pathway activation. *Nat Commun* **13**, 6826, doi:10.1038/s41467-022-34382-7 (2022).

56 Navarro, G. *et al.* Quaternary structure of a G-protein-coupled receptor heterotetramer in complex with Gi and Gs. *BMC Biol.* **14**, 26, doi:10.1186/s12915-016-0247-4 (2016).

57 Yue, Y. *et al.* Structural insight into apelin receptor-G protein stoichiometry. *Nat. Struct. Mol. Biol.* **29**, 688-697, doi:10.1038/s41594-022-00797-5 (2022).

58 Weis, W. I. & Kobilka, B. K. The Molecular Basis of G Protein-Coupled Receptor Activation. *Annu Rev Biochem* **87**, 897-919, doi:10.1146/annurev-biochem-060614-033910 (2018).

59 Bous, J. *et al.* Structure of the vasopressin hormone-V2 receptor-beta-arrestin1 ternary complex. *Sci Adv* **8**, eabo7761, doi:10.1126/sciadv.abo7761 (2022).

60 Sebag, J. A. & Hinkle, P. M. Opposite effects of the melanocortin-2 (MC2) receptor accessory protein MRAP on MC2 and MC5 receptor dimerization and trafficking. *J Biol Chem* **284**, 22641-22648, doi:10.1074/jbc.M109.022400 (2009).

61 Maggio, R., Vogel, Z. & Wess, J. Coexpression studies with mutant muscarinic/adrenergic receptors provide evidence for intermolecular "cross-talk" between G-protein-linked receptors. *Proc Natl Acad Sci U S A* **90**, 3103-3107, doi:10.1073/pnas.90.7.3103 (1993).

62 Zhang, H. *et al.* Structural insights into ligand recognition and activation of the melanocortin-4 receptor. *Cell Res.* **31**, 1163-1175, doi:10.1038/s41422-021-00552-3 (2021).

63 Kay, E. I., Botha, R., Montgomery, J. M. & Mountjoy, K. G. hMRAPa specifically alters hMC4R molecular mass and N-linked complex glycosylation in HEK293 cells. *J Mol Endocrinol* **50**, 217-227, doi:10.1530/JME-12-0220 (2013).

64 Heroux, M., Breton, B., Hogue, M. & Bouvier, M. Assembly and signaling of CRLR and RAMP1 complexes assessed by BRET. *Biochemistry* **46**, 7022-7033, doi:10.1021/bi0622470 (2007).